Final Report

IOMASA

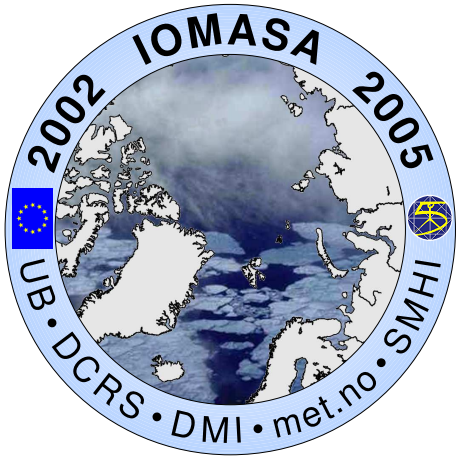

Integrated Observation and Modeling of the Arctic Sea Ice and Atmosphere

Contract Number EVK-CT-2002-00067

1 November, 2002 – 31 October, 2005

G. Heygster, C. Melsheimer, N. Mathew
L. Toudal, R. Saldo
S. Andersen, R. Tonboe
H. Schyberg, F.T. Tveter, V. Thyness
N. Gustafsson, T. Landelius, P. Dahlgren, V. Perov

http://www.uni-bremen.de/~pharos/iomasa

This *Final Report* is a stand-alone version of Section 5 ("Executive Summary") and Section 6 ("Detailed Report, Related to Overall Project Duration") of the contractual final report of the EU project IOMASA.

Main contributors:

Section 3.1 G. Heygster, C. Melsheimer, N. Mathew, H. Schyberg
Section 3.2 H. Schyberg, F.T. Tveter, V. Thyness, N. Gustafsson, T. Landelius, P. Dahlgren, V. Perov
Sections 3.3 and 3.5 L. Toudal, R. Saldo
Section 3.4 S. Andersen, R. Tonboe

The report was compiled and edited by C. Melsheimer

Contents

Executive Summary

Contract n°	EVK-CT-2002-00067	Reporting period:	Nov. 2002 – Oct. 2005
Title	IOMASA – Integrated Observation and Modeling of Arctic Sea ice and Atmosphere		

Objectives: The overall objective of IOMASA was to improve our knowledge about the Arctic atmosphere and ocean by using satellite information which is continuously available, but currently not exploited. This progress was to be achieved through an integrated approach involving

1. Remote sensing of atmospheric parameters temperature, humidity and cloud liquid water over sea and land ice,
2. Improved remote sensing of sea ice with more accurate and higher resolved ice concentrations (percentage of ice covered sea surface), and
3. Improving numerical atmospheric models by assimilating the results of the points 1 and 2.

In addition, the results of the above three fields of activity were to be made accessible to all interested users.

Scientific achievements: An algorithm was developed that retrieves the total water vapour (TWV) content of the atmosphere from data acquired by AMSU-B (Advanced Microwave Sounding Unit B, aboard the polar orbiting satellites of the National Oceanic and Atmospheric Administration, NOAA). For sufficiently dry conditions, fulfilled over most of the Arctic in winter and spring, it is independent of the potentially unknown surface emissivity. An algorithm was developed and tested that retrieves surface emissivity at AMSU-A and -B window channels from AMSU data. It was used to determine typical emissivities of first-year and multiyear ice and to explore the scan angle dependence of surface emissivity.

AMSU-A observations over sea ice were successfully assimilated in HIRLAM 3D-Var (High Resolution Local Area Model, 3-Dim. Variational analysis), and a new approach for estimating microwave sounding channel emissivity over sea ice was developed using information from the EUMETSAT OSI SAF (Satellite Application Facility on Ocean and Sea Ice). A quality control method was developed specifically to handle asymmetric (cloud water) contamination. Assimilating AMSU-A observations over sea ice using the proposed approach had a positive effect on the mean sea level pressure (MSLP) and temperature profiles, especially in northern areas.

The results from the validation of assimilation of TWV retrievals from AMSU-B show that the induced model changes remained in the Arctic region and mainly resulted in better forecasts on temperature, MSLP and geopotential. In addition, validation of TWV assimilation led to the correction of an error in the HIRLAM system.

The development of a new surface heat flux scheme lead to a significant improvement in forecasts of the potential temperature at lower model levels in the cases of moderate and very stable stratification in comparison with the conventional technique. There was also improvement for the vertical profile of wind in the boundary layer, for 2 meter temperature and humidity and for MSLP.

An empirical emissivity model has been established for both the AMSR-E (Advanced Microwave Scanning Radiometer for EOS) microwave frequencies in the range from 6.9 to 89 GHz, and for the AMSU frequencies (23-183 GHz). A microphysical emissivity and backscatter model has been implemented, and used in an extensive evaluation of sea ice concentration algorithms as well as in an assessment of the most important snow parameters influencing the emissivity of the ice/snow surface.

It was found that the sea ice concentration algorithms with the shorter penetration depth, i.e., using mainly 85 GHz information, tend to produce significantly better statistics. During winter it was found that the variability in the reference field was consistently smaller than the variability of the passive microwave retrievals. The results provide a solid basis for the interpretation of sea ice concentration retrievals not only in operational meteorological application that have been the scope of IOMASA, but also in climate and oceanographic applications. The results should have an impact on the future priorities of research. It is recommended to put emphasis on improved knowledge of snow on top of the sea ice and also to pay strong attention to synergies with alternative means of observing the sea ice.
The Internet-based interactive distribution system (browser) provides a wealth of ice/weather and ocean information to all users with Internet access, but can also be used offline.

Socio-economic relevance and policy implications: IOMASA has complemented in an interdisciplinary way expertise and work being done nationally in the fields of (1) remote sensing of the polar atmosphere, (2) modelling and assimilation of the polar atmosphere, and (3) modelling and retrieval of sea ice. It has promoted the scientific cooperation and integration between European universities and research institutes and has contributed to transferring new technologies from research institutes (IUP, DTU) to operational services (DMI, met.no, SMHI). Moreover, it has promoted the cooperation between the involved countries on environmental subjects affecting all of Northern Europe, and helps to improve weather forecasts and sea ice analyses, thus helping to increase prosperity and strengthen security in Northern Europe. It has broadened the European expertise in the fields of (1) remote sensing of the polar atmosphere, (2) atmospheric modelling and assimilation, (3) remote sensing and modelling of sea ice. It also enhances the value of data of European meteorological satellites because sensors similar to the sounders AMSU-A and -B are planned on the future METOP satellites.

Conclusions: The results achieved in IOMASA, will lead to improved numerical weather prediction, in particular over Northern Europe, and to improved ice concentration retrieval/ice charting. They also point out that the snow pack on sea ice is the major unknown for sea ice concentration and type retrieval and needs further research.

Dissemination of Results: It is planned to bring the new assimilation schemes and the improved surface flux scheme into the HIRLAM reference system. Thus it can easily be applied by the weather services of those countries that use local versions of HIRLAM as their operational NWP (numerical weather prediction) system: Denmark, Finland, Iceland, Ireland, the Netherlands, Norway, Spain and Sweden. The work on sea ice emissivity and concentration is taken up by the EUMETSAT OSI SAF. The atmospheric and sea ice parameter fields generated in IOMASA are accessible to all users via the Internet-based interface at http://www.seaice.dk/iomasa

Keywords: Numerical Weather Prediction, Arctic, Remote Sensing Data, Microwave Sounding, Assimilation, Sea Ice Concentration, Surface Emissivity, Total Water Vapour, Cloud Liquid Water

Detailed Report, Related to Overall Project Duration

1 Background

At present, the polar regions belong to the regions of which the least information is available about the current and predicted states of surface and atmosphere. Because of sparse observations, we only have at a rough quality weather forecasts for northern Europe, and ice charts for the ice frequented waters of the European Arctic.

2 Scientific/technological and socio-economic objectives

The objective of IOMASA was to improve our knowledge about the Arctic atmosphere by using satellite information which is continuously available, but currently not optimally exploited. The approach was an integrated one involving the following four components

1. Remote sensing of the atmospheric parameters humidity, cloud liquid water and temperature over sea and land ice.
2. Improved remote sensing of sea ice with more accurate and higher resolved ice concentrations (percentage of ice-covered sea surface).
3. Improving numerical weather prediction (NWP) models by assimilating the results of components 1 and 2.
4. In order to prove the usefulness of this concept, a real time processing set-up and a user interface was set up.

A detailed description follows:

Remote sensing of atmospheric parameters over sea ice A recently proposed procedure to retrieve the total water vapour in the range of 0 to 6 kg/m^2 over Antarctic sea and land ice from data of the microwave humidity sounder SSM/T2 (Special Sensor Microwave/Temperature sounder 2) was to be adapted (1) to the similar sensor AMSU-B (Advanced Microwave Sounding Unit; part of ATOVS aboard the polar orbiting satellites of the National Oceanic and Atmospheric Administration, NOAA) and (2) to Arctic conditions.

Fields of the cloud signature (roughly the cloud liquid water) were to be derived from SSM/I (Special Sensor Microwave/Imager) data after adapting the method (originally derived for the Antarctic) to Arctic conditions.

A method to improve the retrieval of temperature profiles from microwave sounders working in the oxygen absorption band near 60 GHz (e.g., AMSU-A, SSM/T1) by including surface emissivity information in regions (partially) covered by sea ice was to be adapted to direct assimilation and Arctic conditions.

Remote sensing of sea ice. For large-scale remote sensing of sea ice, passive microwave sensors offer the unique features of independence of darkness (polar night), nearly independence of cloud cover and daily global coverage. Operational products mainly relied on the SSM/I with data available since over 20 years ago. The combined use of active and passive microwave sensors has been little explored, mainly due to the narrow swath of the ERS (European Remote sensing Satellite) scatterometers and the early failure of NSCAT (NASA SCATterometer) aboard ADEOS (Advanced Earth Observing Satellite). However, with the advent of the SeaWinds scatterometer aboard QuikSCAT (1999), scatterometry-based sea ice detection has gained momentum and obvious synergies with passive microwave instruments particularly regarding ice type detection have emerged.
Furthermore, two new, almost identical passive microwave instruments, AMSR (Advanced Microwave Scanning Radiometer) aboard ADEOS-2 and AMSR-E aboard the Aqua satellite have been launched in 2002. Their channels include all SSM/I channels, but at much higher resolution.
This project aimed at developing and testing a set of improved algorithms to derive ice concentration from active and passive microwave satellite data with high temporal repetition using the best available information from other sources to correct for the unwanted/unknown parts of the signals (in parenthesis the source of correction information): (1) cloud liquid water (cloud signature from SSM/I), (2) atmospheric water vapour (improved NWP short term predictions), (3) wind speed over open ocean (NWP, SSM/I and scatterometers), (4) ice surface temperature (short term NWP results plus relaxation for surface temperature changes), and (5) ice surface emissivity (empirical ice evolution models).
Past attempts to derive ice concentrations primarily relied on the microwave radiometer signals itself to correct for these effects, the remaining uncertainty being in the order of 5...10%, sometimes up to 30%. The aim was to reduce these numbers substantially using auxiliary information from short term numerical weather prediction, supplementary satellite sensors and algorithms, and an improved knowledge of the temporal and spatial variability of the ice surface signatures.
The errors of the ice concentration algorithms are assessed by thorough comparison to classified SAR data, ship observations and information derived from high resolution observed sea ice dynamics.

Improving numerical atmospheric models

(1) Assimilation of atmospheric parameters into NWP models. A significant part of the forecast errors in numerical weather prediction comes from errors in the initial state, and in particular from the lack of observations of the atmospheric state in remote areas over the oceans and polar ice caps.
The use of satellite sounding data from microwave and infrared channels from the ATOVS sensor package (including AMSU-A and AMSU-B) has contributed to relieving this problem over open ocean. Radiances measured by these instruments play an important role in the meteorological observing system. They are intensively used by many NWP centres. Over sea and land ice, however the use of ATOVS channels has been limited.
A main goal in this project was to improve atmospheric models over and near the Arctic by enhanced use of AMSU-A temperature sounding observations and by taking AMSU-B moisture sounding data into use over ice[1]. An optimal treatment of the AMSU-A and AMSU-B data in assimilation was to

[1]It was planned to also consider extending the methods to data from the new sensor SSMIS (scheduled for launch in November 2001). This sensor has the advantage of simultaneous soundings of temperature and humidity, and sea ice detection. However, the launch was delayed until late 2003, and for various reasons, until the end of the project, practically no SSMIS data were available.

be found, applying estimates of ice concentration and surface emissivity. This would lead to more efficient data assimilation of sounding data over ice in general, and to improving weather forecasts over the Arctic when applied in a high-resolution limited-area model.

(2) Improved surface heat flux modelling. A closed sea ice cover reduces the heat flux up to two orders of magnitude, with small openings contributing significantly to the atmospheric heat budget. The effect of a surface heat flux parameterisation using ice concentrations from a SSM/I or multi-sensor retrieval in terms of the effect on forecast quality was to be studied.

For both types of improvements, special emphasis was put on obtaining impact of the data in high-resolution limited-area models, here with horizontal resolution of 20 km or better. Limited area models are continuously forced by the lateral boundary conditions (with values usually taken from a coarser, typically global, NWP model). There is a potential for improving the (especially short-range) forecast skill by better estimates of the initial state. In particular the higher density of satellite passages at the high latitudes could be exploited, where the gaps between the conventional observations are large. The results were to be validated in parallel forecast cycle experiments.

User interface The results of the above three fields of activity were to be brought directly to all interested users via a web-based interface.

3 Applied methodology, scientific achievements and main deliverables

The IOMASA consortium consisted of 5 partners:

1. Institute of Environmental Physics (in German: Institut für Umweltphysik), at the University of Bremen, Germany – IUP
2. Danish Remote Sensing Centre of Technical University of Denmark – DTU
3. Danish Meteorological Institute – DMI
4. Norwegian Meteorological Institute met.no
5. Swedish Meteorological and Hydrological Institute – SMHI

According to the objectives, IOMASA was structured into five parts, for each of which one or two partners from the IOMASA consortium took the main responsibility:

Part 1: Remote sensing of atmospheric parameters (IUP),
Part 2: Improving numerical weather prediction models (met.no, SMHI),
Part 3: Empirical model for emissivity and backscatter of sea ice (DTU),
Part 4: Sea ice concentration retrieval (DMI),
Part 5: Demonstration of real time processing and user interface (DTU)

3.1 Part 1: Remote sensing of atmospheric parameters

3.1.1 Total water vapour retrieval with AMSU-B

While AMSU-B is designed and operationally used for humidity sounding, this fails over polar regions since there, (1) the total water vapour content of the atmosphere is so low that the contribution caused by surface emission is substantial and (2) the surface emission is poorly known and highly variable because of variable ice cover of the seas. The method described in the following which retrieves total water vapour (TWV) is complementary in that it works exactly where the atmosphere is dry enough for the ground to be ”seen” by the sensor, and it is mostly independent of the surface emissivity.

Table T-2: *AMSU-B channels and frequencies*

Freq. [GHz]	89.0	150.0	182.31±7	182.31±3	182.31±1
AMSU channel	16	17	20	19	18

Basic Algorithm The original algorithm retrieving total water vapour (TWV, also total precipitable water or total column water vapour) mainly from SSM-T2 was developed for Antarctic conditions by Miao [1998]; Miao et al. [2001]. In IOMASA, it was first adapted/reimplemented for use with AMSU-B data and Arctic conditions. Then, the algorithm was extended so that it can retrieve TWV contents above about 7 kg/m^2 (the upper limit of the original algorithm).
The algorithm relies on the brightness temperature measured in the three water vapour channels (channels 20, 19, 18 of AMSU-B, see Table 3.1.1 for the channels), or in the window channel at 150 GHz (channel 17) and the two less sensitive water vapour channels (channels 20 and 19). Under the condition that the surface emissivities at all three channels used are about the same, the total water vapour can then be retrieved, independent of the surface emissivity, in the following way:

$$TWV \sec\theta = C_0 + C_1 \ln\left(\frac{T_{b,i} - T_{b,j} - F_{ij}}{T_{b,j} - T_{b,k} - F_{jk}}\right) \tag{1}$$

where θ denotes the looking angle (scan angle), i, j, k denote three AMSU-B channels used, $T_{b,i}$ is the brightness temperature measured at channel i etc., and C_0, C_1, F_{ij}, and F_{jk} are calibration parameters that are determined with a regression method based on radiosonde data and simulated AMSU-B brightness temperatures. For the simulation, the Atmospheric Radiative Transfer Simulator [ARTS, see Buehler et al., 2005] was used. Using channels 20, 19 and 18 (i.e., $(i,j,k) = (20,19,18)$), and channels 17, 20 and 19 ($(i,j,k) = (17,20,19)$), TWV values up to about 6 to 7 kg/m^2 can be retrieved. Careful mathematical and physical analysis showed that:

- the condition when the algorithm is not applied any more (saturation) can be relaxed from originally
  $T_{20} - T_{19} \geq 0$ ("saturation cut-off" = 0)
  to
  $T_{20} - T_{19} \geq F_{20,19}$ ("saturation cut-off" = $F_{20,19}$)
  where $F_{20,19}$ is typically a few K
- as long as both numerator and denominator of the log argument are negative, the algorithm works.

$$\log \frac{T_{b,i} - T_{b,j} - F_{ij}}{T_{b,j} - T_{b,k} - F_{jk}}$$

This has increased the range of retrievable values.

Extension of the algorithm to higher TWV values If the TWV is above about 6 to 7 kg/m^2, channel 19 becomes saturated, and the algorithm sketched above does not work any more. We therefore have to re-derive the algorithm, starting from the same point as for the standard algorithm, but with the following relaxed premises:

- The channels i, j, k denote AMSU-B channels 16 (89 GHz), 17 (150 GHz), and 20 (182 ± 7 GHz), respectively.
- For the surface emissivities $e_i \neq e_j$, $e_j = e_k$
- Still valid: $\kappa_i < \kappa_j < \kappa_k$

We then get:

$$W \sec\theta = C_0 + C_1 \log\left(\frac{r_j}{r_i}\left[\frac{T_i - T_j - F_{ij}}{T_j - T_k - F_{jk}} + C\right] - C\right) \tag{2}$$

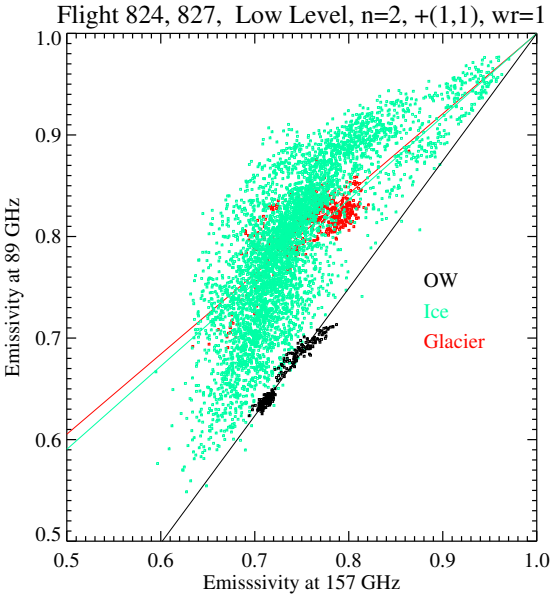

Figure F-1: *Scatter plot of emissivities at 89 and at 157 GHz, from SEPOR/POLEX data. Black: open water (OW), green: sea ice, red: land ice (on Svalbard).*

Here, $r_i = 1 - e_{89}$ and $r_j = 1 - e_{157}$ are the surface reflectivities, C (the term mentioned above that is a function of zenith opacities) depends on the water vapour absorption coefficients but can safely be approximated by 1 for TWV above 6 kg/m^2. We shall call the ratio r_j/r_i reflectivity ratio.
The needed emissivity data were taken from the measurement campaign SEPOR/POLEX [see Selbach, 2003] that took place in the Arctic in winter. The data show that the emissivities at 150 and 89 GHz over water and over sea ice are correlated, cf. Figure F-1. A linear regression yields $e(89)$ as a function of $e(157)$:

$$e_{89} = a + be_{157} \tag{3}$$

The regression was constrained in such a way that $e_{89}(e_{157} = 1) \approx 1$ which results in $a + b \approx 1$ and thus, for the reflectivity ratio,

$$r_j/r_i = \frac{1}{b} \tag{4}$$

For the data measured over sea ice, the regression resulted in

$$a = 0.1809 \tag{5}$$
$$b = 0.8192 \tag{6}$$

Whereas for the retrieval only the reflectivity ratio is needed, which is approximated by the constant $1/b$, the full functional relationship $e_{89} = a + be_{157}$ has to be used for the AMSU-B T_b simulation calculations which are needed to get the four calibration parameters, C_0, C_1,F_{ij}, F_{jk}. The same procedure can also be used with the reflectivity ratio for open water in order to retrieve TWV over open water. However, our main focus was to retrieve water vapour over ice because this is what is new (there are other, well-known methods to retrieve TWV over open water, e.g., from SSM/I data).
An example map of the TWV over the Arctic, retrieved from AMSU-B data with the extended algorithm is shown in Figure F-2 (left panel). For comparison, a TWV map from NCEP (National Centers for

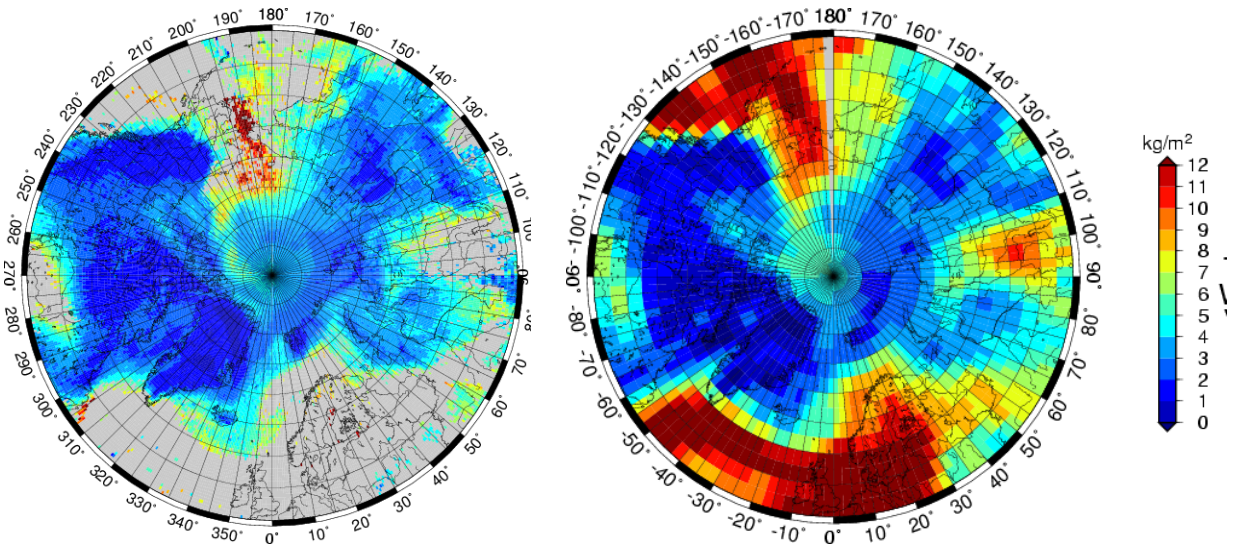

Figure F-2: *Maps of TWV over the Arctic. Comparison of (left:) TWV retrieved from AMSU-B data with the extended algorithm and (right:) TWV from reanalysis data of NCEP (National Centers for Environmental Prediction). 18 March, 2002. Note the intrusion of moist air (TWV>10kg/m^2) through the Bering Strait (between centre and upper edge of the maps).*

Environmental Prediction) for the same day – 18 March, 2002 – is shown in the right panel. Note the intrusion of moist air (TWV>10 kg/m^2) through the Bering Strait (between centre and upper edge of the maps). With the standard algorithm, such high TWV values could not have been retrieved.

Validation of the algorithm The weighting functions of the AMSU-B channels as a function of total water vapour (TWV) in Figure F-3 show roughly at which TWV values a channel is sensitive to water

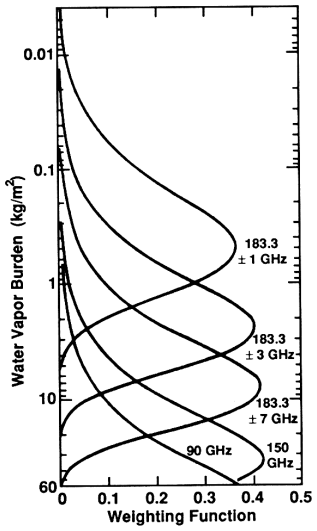

Figure F-3: *Weighting functions of AMSU-B channels as a function of total water vapour ("water vapour burden") over land, from Janssen [1993]*

vapour. For example, the channel at 183.3±1 GHz (channel 18) is sensitive for TWV up to about 2 kg/m^2. For higher TWV, the weighting function rapidly approaches zero, in which case the channel is said to be

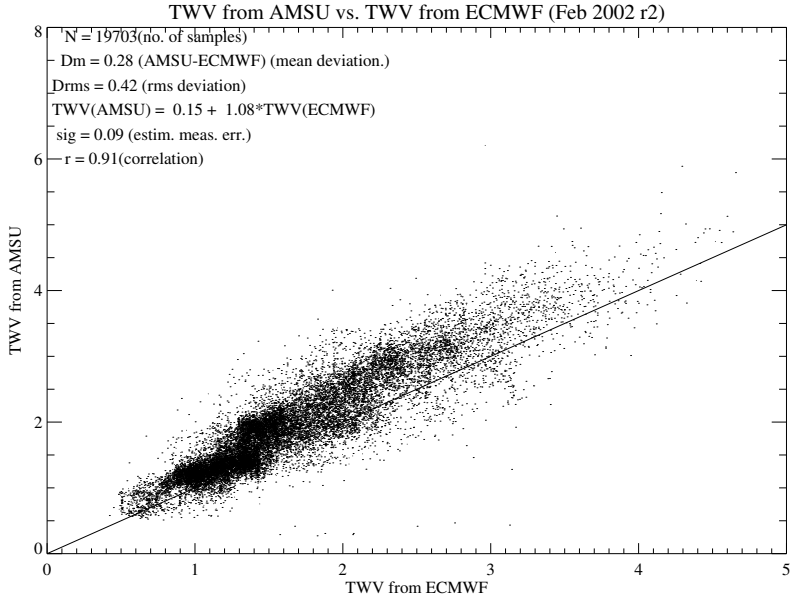

Figure F-4: *AMSU-B-derived TWV versus ECMWF (ERA-40) TWV. February 2002, North of Greenland (83–90° N, 0–90° W); solid line = identity.*

saturated – thus, if there is so much water vapour that a channel is saturated, the radiation that the sensor measures does not come from the whole atmosphere any more, but only from an upper portion (the channel "does not see the surface any more"). Channel 19 (183.3±3 GHz) saturates at around 8 kg/m^2 TWV (which roughly corresponds to the upper limit of the standard algorithm), channel 20 (183.3±7 GHz) saturates at around 20 kg/m^2 TWV - so we can expect the extended algorithm to retrieve water vapour roughly up to that value.

For validation purposes, the TWV data retrieved from AMSU-B data were compared to collocated ECMWF (European Centre for Medium-Range Weather Forecasts) reanalysis (ERA-40) data. For a typical winter month, February 2002, the result is shown in Figure F-4. The correlation is 0.91, and the bias, i.e., the mean difference AMSU-derived minus ECMWF-reanalysis TWV, is about 0.31 kg/m^2. As seen in the plot, most TWV values are below 7 kg/m^2, so the standard algorithm has been used which is independent of surface emissivity.

The same comparison, but for a late summer month, August 2002, with minimum sea ice cover, is shown in Figure F-5. Here, all values above 7 kg/m^2 have been retrieved using the extended algorithm. The correlation is only moderate, and the mean difference is much higher, about 2.7 kg/m^2. The reason is, of course, that the constant reflectivity ratio based on the regression analysis of SEPOR/POLEX data is only an approximation.

Comparison with TWV data derived from radiosonde measurements during Polarstern cruises is difficult since there are very little concurrent data, except for the cruise ARK XIX-1 (March-April 2003). The result of this comparison is shown in Figure F-6. Here, the bias is positive as well, 1.3 kg/m^2, i.e., the AMSU-derived TWV values are higher than the ones derived from the radiosonde measurements. At least part of this positive bias can be explained by the fact that the radiosonde type used on Polarstern is Vaisala RS80. This radiosonde type is known to have a dry bias in cold conditions [Elliot and Gaffen, 1991], i.e., it then underestimates humidity.

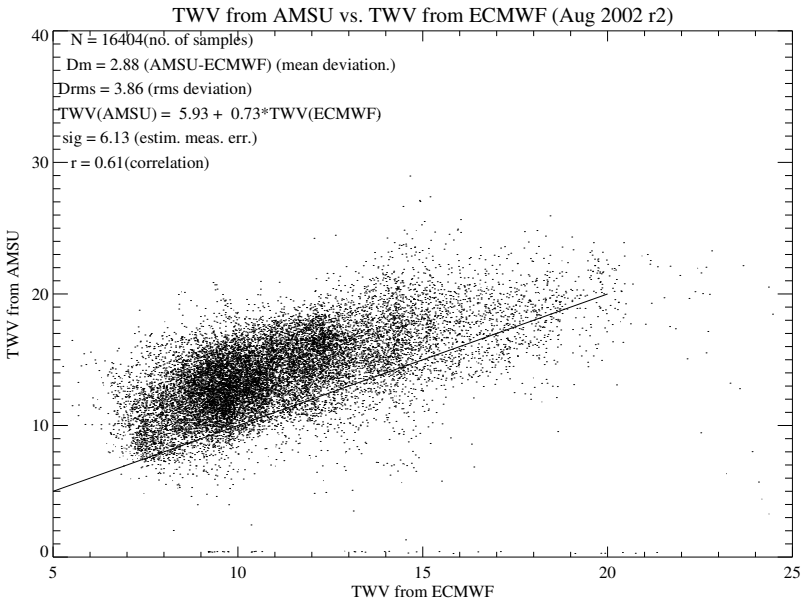

Figure F-5: *AMSU-B-derived TWV versus ECMWF (ERA-40) TWV. August 2002, North of Greenland (83–90° N, 0–90° W); solid line = identity.*

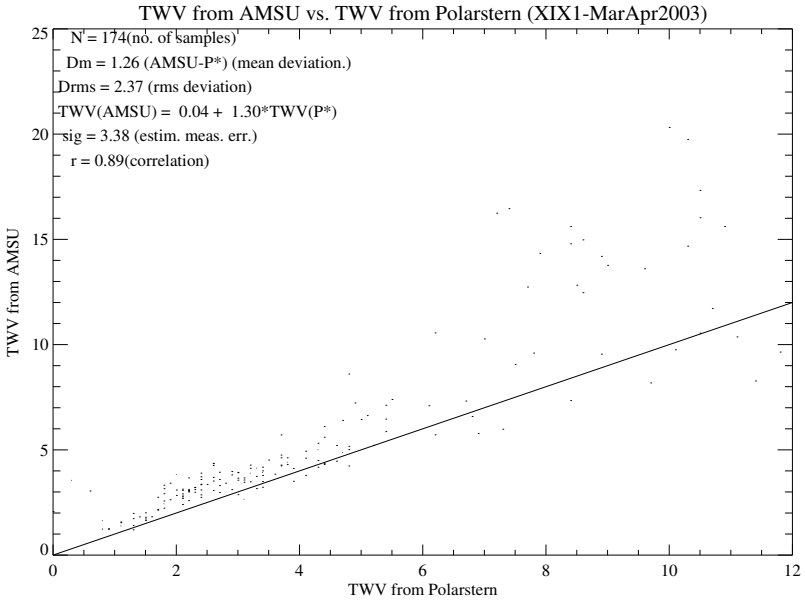

Figure F-6: *AMSU-B-derived TWV versus Polarstern radiosonde TWV, March-April 2003 (cruise ARK XIX-1); solid line = identity.*

3.1.2 Emissivity at temperature-sounding frequencies

Knowledge of the temperature profile of the atmosphere is of critical importance in climatological and meteorological studies. Data from the AMSU-A radiometer are well suited for the continuous retrieval of temperature profiles in polar regions. Since in these regions, the surface is highly variable (open water, various ice types), it is essential to approximately know the emissivity for all possible scan angles and all window channels of AMSU-A in order to estimate the surface contribution to the brightness temperature measured by the satellite. The surface emissivities retrieved from AMSU-A data as described in the following can then be used in the temperature retrieval according to the methods described by Miao et al. [1995] and Rosenkranz [2001].

Surface emissivity algorithm Starting point for the algorithm for deriving surface emissivity from satellite radiometer data is the total brightness temperature measured by that radiometer, e.g., AMSU-A (viewing angle θ, frequency ν) is:

$$T_b(\theta,\nu) = c_1 + c_2 e T_s + (1-e)c_3 \tag{7}$$

where

c_1 $= T_u(\nu,\theta)$, upwelling radiation from atmosphere
c_2 $= \mathrm{e}^{-\tau(0)\sec\theta}$, $\tau(0)$ = opacity of atmosphere
c_3 $= T_d(\nu,\theta)\mathrm{e}^{-\tau(0)\sec\theta}$, downwelling radiation from atmosphere
T_s = physical temperature of the surface
e =emissivity of the surface

Solving the above equation for the surface emissivity e yields

$$e = \frac{T_b - c_1 - c_3}{c_2 T_s - c_3} \tag{8}$$

From (7) we get

$$T_b(e=0) = c_1 + c_3 \tag{9}$$
$$T_b(e=1) = c_1 + c_2 T_s \tag{10}$$

Substituting (9) and (10) into (8) yields

$$e = \frac{T_b - T_b(e=0)}{T_b(e=1) - T_b(e=0)} \tag{11}$$

where $T_b(e=0)$ and $T_b(e=1)$ are simulated brightness temperatures for the hypothetical surface emissivities 0 and 1, using the radiative transfer model MWMOD [MicroWave radiative transfer MODel Fuhrhop et al., 1998], and atmospheric profiles from ECMWF reanalysis data. This means that the surface emissivity at AMSU-A window channels can be derived from the corresponding measured brightness temperatures with the aid of atmospheric profiles and a radiative transfer model. Note that this algorithm can also be applied to the window channels of AMSU-B.

Validation In order to validate the emissivity algorithm, retrieved emissivities over open water were compared with modelled emissivities: The microwave emissivity of open water is well known (provided the wind speed and water temperature are known), here we used the state-of-the-art model FASTEM [Fast Emissivity Model, see English and Hewison, 1998]. The needed wind and temperature information for

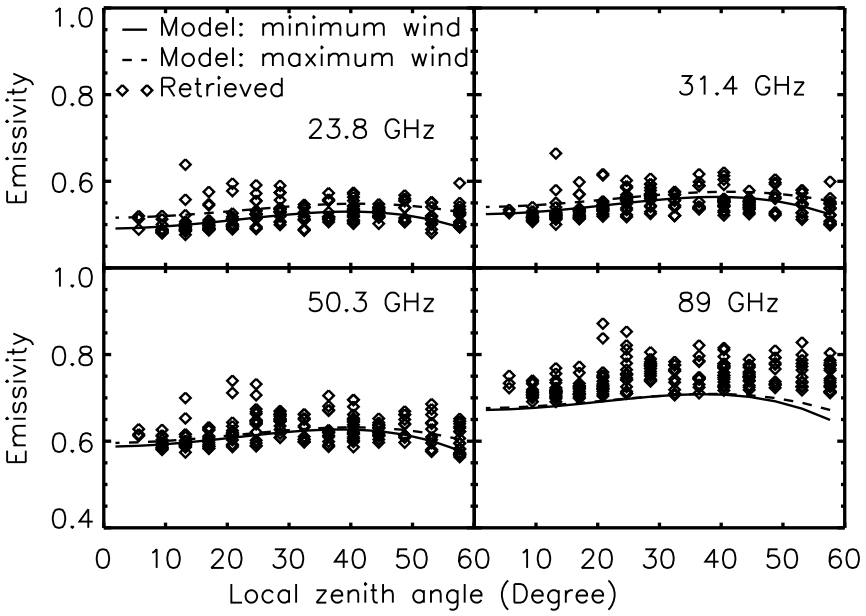

Figure F-7: *Emissivity of open water from AMSU-A/Polarstern profiles (symbols) and from FASTEM (lines); Arctic, all AMSU-A window channels; wind: 6.3 m/s, 16.8 m/s*

FASTEM as well as the atmospheric profiles for the emissivity algorithm were taken from concurrent, colocated data measured during a Polarstern cruise.
Figure F-7 shows both modelled and retrieved emissivities as a function of local zenith angle; the solid and the dashed lines represent the modelled emissivities for the lowest and highest measured wind speed, 6.3 m/s and 16.8 m/s, respectively, with corresponding sea surface temperatures of 271.0 K and 274.7 K; the symbols represent the emissivities retrieved from AMSU data. Modelled and measured data agree well for the lower three channels, the scatter of the retrieved data is probably caused by differences within the – temporal and spatial – collocation window. At 89 GHz, the retrieved data seem to have a positive bias. It is the channel that is most sensitive to atmospheric influences, e.g., high water vapour content.

Results

Dependence on looking angle The AMSU instruments measure in linear polarisation with an orientation angle that depends on the scan angle [Weng et al., 2003]. If θ_s is the scan angle and θ_z is the local zenith angle, then the surface emissivity e for AMSU-A window channels that is "seen" by the AMSU-A instrument can be written as

$$e(\theta_z) = e_v(\theta_z)\cos^2(\theta_s) + e_h(\theta_z)\sin^2(\theta_s) \tag{12}$$

where e_v and e_h are the vertically and horizontally polarised surface emissivities, respectively. Since in general (for plain Fresnel emissivities as well as for more realistic models), e_v increases with incidence angle while e_h decreases, this compensates the decreasing of the cosine square and the increasing of the sine square up to a local zenith angle of about 45°. This can be seen from modelled and retrieved AMSU emissivities of open water, see Figure F-7 above, and was also confirmed for retrieved emissivities of ice (not shown here). Thus, up to $\theta_z = 45°$, the incidence angle dependence of the emissivity relevant for AMSU-A is negligible.

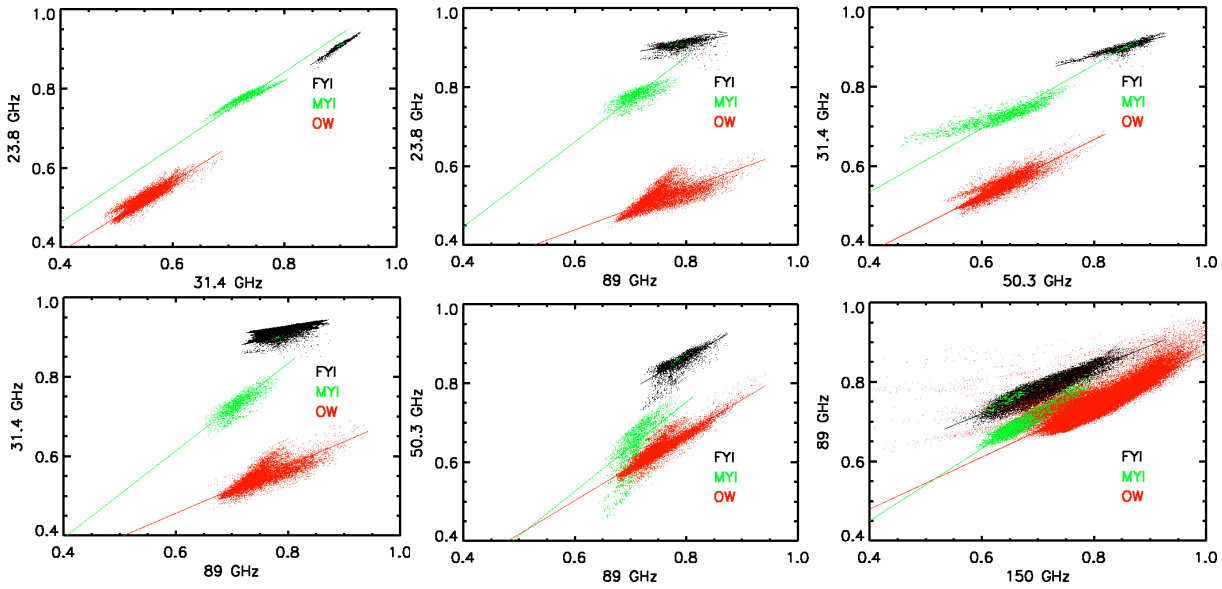

Figure F-8: *Scatter plot of emissivities at several frequency pairs, for three different surface types: First-year ice (black), multiyear ice (green), and open water (red). Average of March 2005.*

Relation between emissivities at different frequencies Being able to retrieve emissivities for the AMSU window channels, we can explore the relation of emissivities for different frequencies and surface types. Therefore, emissivity was retrieved for regions with known surface types: open water, first-year ice (FYI), multiyear ice (MYI). Figure F-8 shows scatter plots of retrieved emissivities for several frequency combinations, with different colours for the three different surface types. We can see that for the lower two channels, i.e., at 23.8 and 31.4 GHz, the emissivities of open water, FYI and MYI hardly overlap (cf. top left plot). At 50.3 GHz, FYI and MYI emissivity cannot be separated any more, but the overlap with open water emissivity is negligible (cf. top right and bottom centre plot). At 89 and 150 GHz, the three surface types cannot be separated (cf. bottom centre, bottom right plots).

Emissivity maps With the emissivity algorithm, we can produce emissivity maps with a grid size of about 1° in latitude and longitude. Figure F-9 shows such maps of the Antarctic for all the window channels of AMSU-A and AMSU-B, averages over one day (April 25, 2002) for all scan angles below 36.4°. The lower frequencies better differentiate different surfaces, e.g., low emissivity regions as open ocean, high emissivity regions as sea ice and the moderate emissivity region as land ice. As the frequency increases, the atmospheric influence on the emissivity calculation increases as well. Some snow covered low emissivity regions on the Antarctic continent are also observed. The 89 GHz channels on both AMSU-A and AMSU-B within a certain local zenith angle range behave similarly, as expected.

3.1.3 Monitoring the Arctic Atmosphere with cloud signature products

Background One of the main goals of the IOMASA project is to improve Arctic weather forecasting. In this section we describe another type of product, the so-called R-factor cloud imagery [Miao et al., 2000] which can be made available for duty forecasters for their subjective analysis and nowcasting.
Moisture, clouds and precipitation observations are not as well assimilated in present assimilation systems as one could wish. Clouds and precipitation are among the features usually used for identifying fronts by operational forecasters. This allows forecasters to identify areas of interesting weather and active weather developments as well as monitor the performance and accuracy of the numerical weather

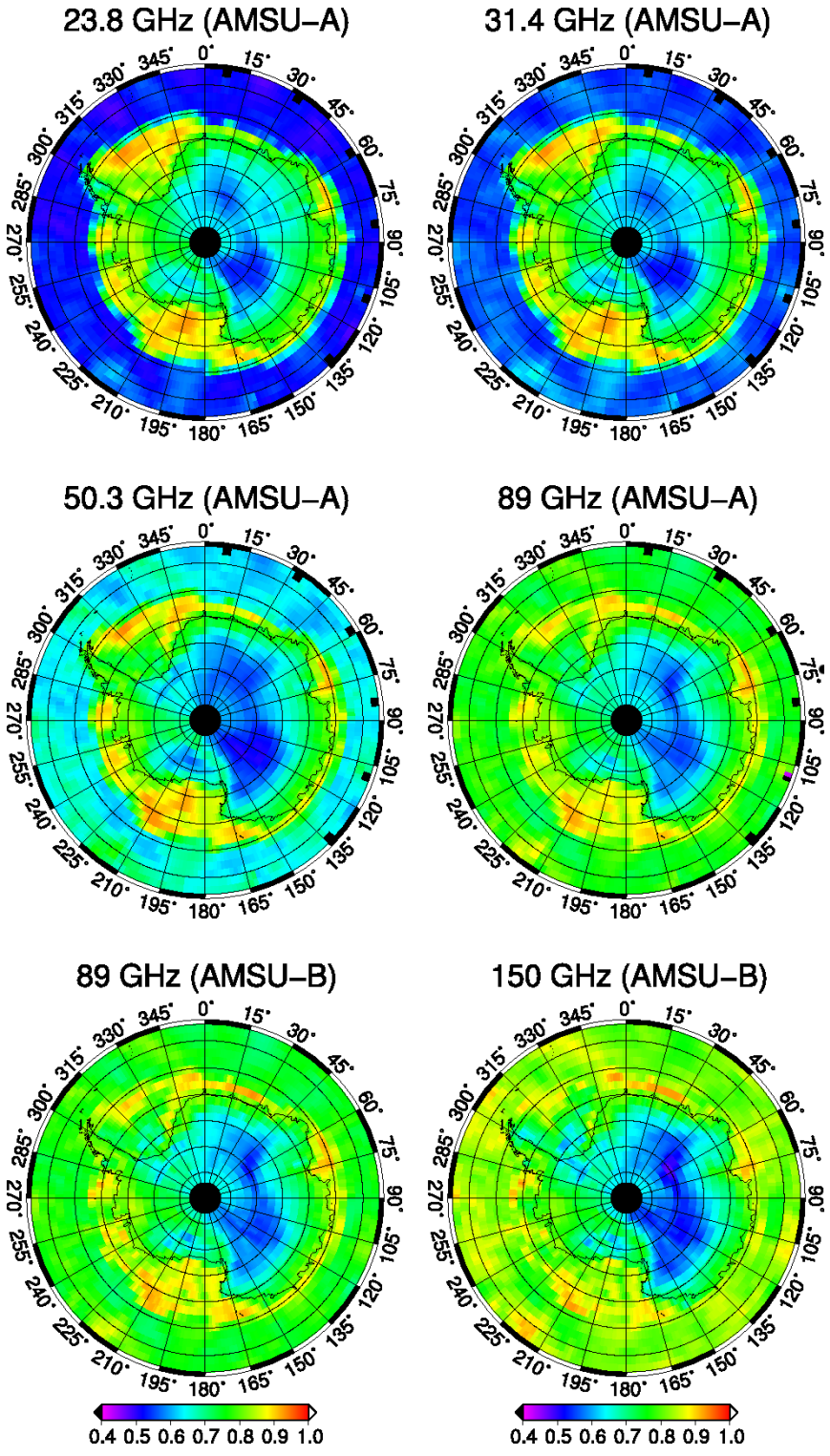

Figure F-9: *Maps of the emissivity of Antarctic for all AMSU window frequencies, 25 Apr 2002*

prediction (NWP) models.

The art of assimilating precipitation, cloud and moisture is still not a very mature science, for instance it is difficult to develop a satisfactory assimilation system giving feedback from cloud or precipitation field back to wind and mass fields. If such a method were available, that would be an ideal situation which for instance could allow the assimilation scheme to move fronts in a consistent way. Because of these limitations there is still room for subjective analysis by weather forecasters using moisture and cloud information to add some value to the numerical forecast on short forecasting ranges, because these observations are still not be well exploited in NWP.

The background theory and motivation for introduction of the "R-factor" is described in Miao et al. [2000]. The idea was to use polarisation differences at the two high frequency channels of the Special Sensor Microwave Imager (SSM/I) to use this quantity to detect cloud signatures under certain conditions.

Theoretically the R-factor can be shown to be a sum of two terms, one representing the ground surface signal and the other representing the contribution of total cloud liquid water (TCLW) and the atmospheric water vapour. It his here assumed that the TCLW term is the dominant contribution over open ocean.

Results and recommended application In Figure F-10 shows AMSU-A (Advanced Microwave Sounding Unit) imagery as well as R-factor imagery presented together with NWP pressure and total cloud liquid water (TCLW) model output from HIRLAM (High-Resolution Limited Area Model). We see that there is good match between all three cloud liquid water products in shapes and intensities.

Several other examples with both AMSU-A TCLW imagery and HIRLAM TCLW forecast fields throughout the investigation period have been studied, and in general the R-factor seems a reliable indicator of column cloud liquid over ocean.

We see that the SSM/I R-factor products clearly add details by having better spatial resolution than the AMSU-A TCLW product. It also adds coverage, having wider swaths. It is generally seen in the investigation period that the number of DMSP (Defense Meteorological Satellite Program) satellites and swath width gives more coverage than AMSU-A, and it complements the AMSU data coverage in a nice way.

Figure F-11 shows a weather situation where the forecaster's analysis closely matches a short-range forecast output from HIRLAM. There is a low pressure system east of Iceland, and probably few observations in the area to help the forecaster locate any front. We see that it follows closely the position which would be depicted by for instance the precipitation output from the model. If we look at the R-factor imagery (lower panel), we see clearly, however, that the occluded front is misplaced and should be further back. Looking at R-factor imagery from earlier the same day, we also found a consistent misplacement of the occluded front in earlier analyses.

The secondary fronts depicted by the forecasters are also of different shape and position than indicated, if one looks for lines of high cloud water in the R-factor imagery.

This is just one of many similar examples which was seen during the period of the availability of this product. Several could have been presented, and the impression is that this imagery can be a useful tool in locating fronts. We have also seen examples showing waves on fronts indicating new low pressure system developments in the R-factor imagery, where these waves have not been found in the forecaster's analysis. Such waves often occur in areas in the Northeast Atlantic with sparse conventional observation coverage. Availability and use of these data by forecasters in these ocean regions would therefore have significant potential usefulness.

The R-factor cloud water imagery complements other data sources such as radar imagery and AMSU-A TCLW imagery well. It adds information over ocean areas where the only other major observational source of total column liquid water data is AMSU-A imagery. It has, however, higher resolution than AMSU-A, giving more details in fronts and weather systems. On the other hand it it not a quantitative measure, but this is not crucial for the use by operational forecasters. It can be an important tool in

identifying low pressure developments over open ocean areas and for identifying misplaced fronts in the numerical weather prediction model products.
If the subjective analysis performed by operational weather forecasters should have any role and add something to numerical forecasts, one way of doing that is to identify errors, weather system displacements or deficiencies in the numerical forecasts. R-factor imagery is clearly a tool which can help with this. There is still no mature method for assimilation of such imagery, so in this respect this is the only way the information contained in the R-factor product can be well used.
The use of the R-factor is, however, of little help over large areas of closed sea ice in the Arctic ocean. The areas in the marginal ice zone with sufficiently small ice concentrations to enable use of the product, are generally too small to be of any significance.
Given the quality, resolution and usefulness of the R-factor imagery, it is recommended to exploit the possibility of making the SSM/I data available more timely, and to make these images available for the operational forecasters. Land and sea ice should be masked out and duty forecasters should be educated on the use of these images.

3.2 Part 2: Improving numerical weather prediction models

The purpose of this project part was to improve NWP by enhanced use of AMSU-A and AMSU-B data, namely by assimilation of total water vapour (TWV) data over ice, derived from AMSU-B, and/or assimilation of AMSU-A and AMSU-B radiances over ice. Assimilation of AMSU-A data was dealt with by met.no while assimilation of AMSU-B and humidity (TWV) data was dealt with by SMHI. Furthermore, SMHI worked on an improved surface flux modelling together with the use of ice concentration measurements.

3.2.1 Use of AMSU-A data

In IOMASA, the project partners have developed processing methods to enable beneficial use of AMSU-A observations over sea ice. AMSU-A is assimilated in the present version of the HIRLAM 3D-Var assimilation system at met.no, but is only used over ocean [see Schyberg et al., 2003]. A potential is foreseen in these observations in sea-ice covered Arctic areas where few other observations are available.
An important component in the system for assimilating AMSU-A observations in HIRLAM 3D-Var, is the 'forward model', RTTOV [Radiative Transfer for TOVS, see Saunders and Brunel, 2002]. The forward model simulates the AMSU-A observations using a model representation of the atmosphere, and the data assimilation system then tries to optimally adjust the HIRLAM representation of the atmosphere so that the RTTOV simulated radiance observations better agree with the observed radiances.
For AMSU-A channels that are sensitive to the surface, the RTTOV forward model requires an estimate of the emissivity of the surface. The error in the forward model in channels that are sensitive to the surface emissivity, decreases as the emissivity estimate improves. Simple, yet very successful, AMSU-A emissivity models depending on surface wind speed are available for open sea [English and Hewison, 1998]. Unfortunately, the nature of sea ice surfaces is such that emissivity depends on the history of the sea ice, and has proven to be more difficult to model in a simple way.
On the other hand, the sea ice emissivity properties have some stability in time, and first-year and multi-year ice have distinctly different emissivities. Thus, in this work we exploit daily sea ice charts showing first-year and multiyear sea ice concentration retrievals from an experimental version of the Ocean and Sea Ice Satellite Application Facility (OSI SAF) processing chain [Breivik et al., 2001].
Another difficulty in setting up an assimilation scheme for AMSU-A over sea ice lies in identifying observations contaminated by clouds. RTTOV simulates AMSU-A observations in clear sky conditions,

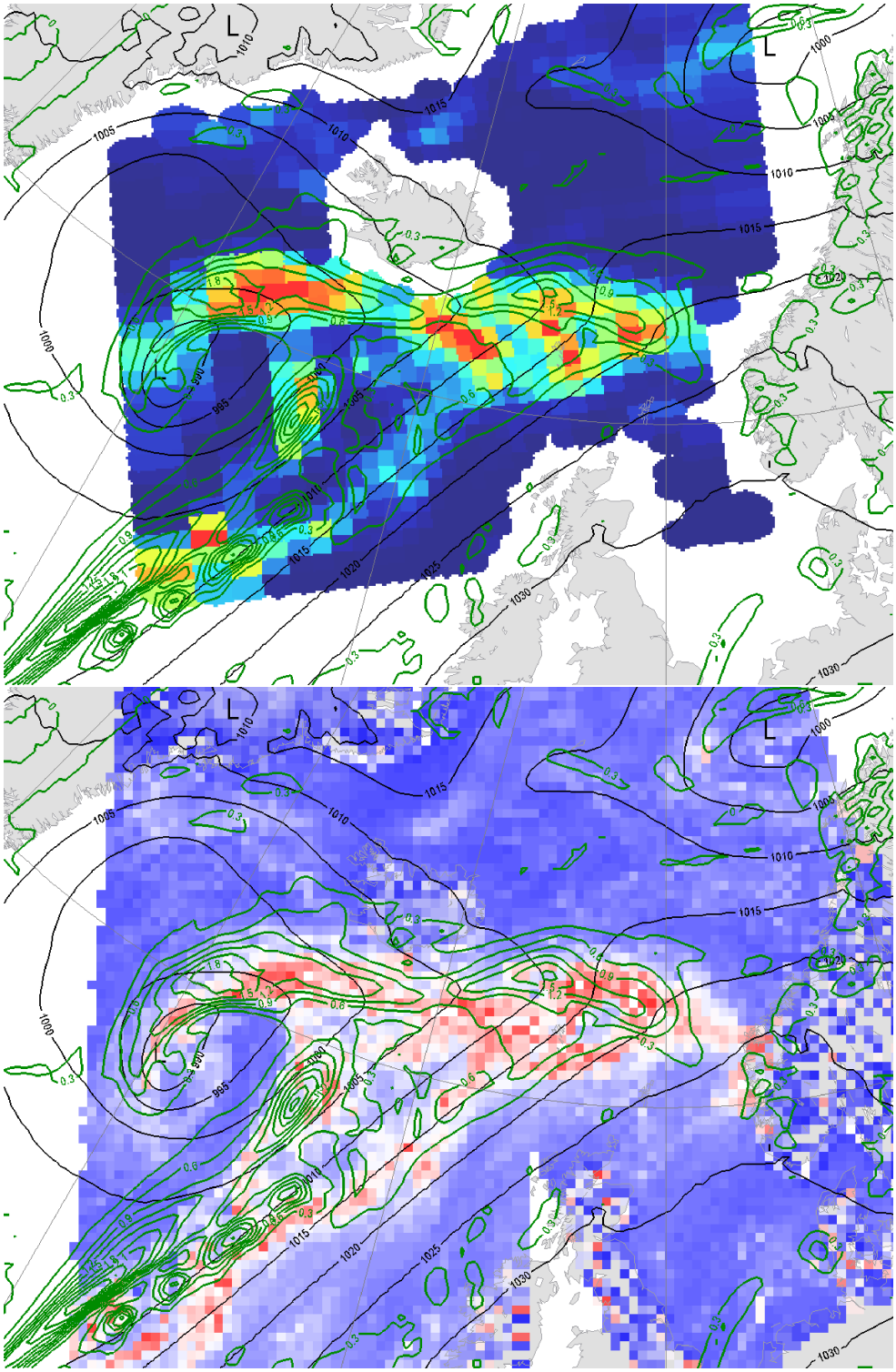

Figure F-10: *Weather situation on 3 October 2005, 18UTC. Upper panel: AMSU-A TCLW imagery with overlaid HIRLAM pressure analysis analysis and a short-range TCLW forecast. Lower panel: As above, but with R-factor imagery instead of AMSU-A TCLW imagery.*

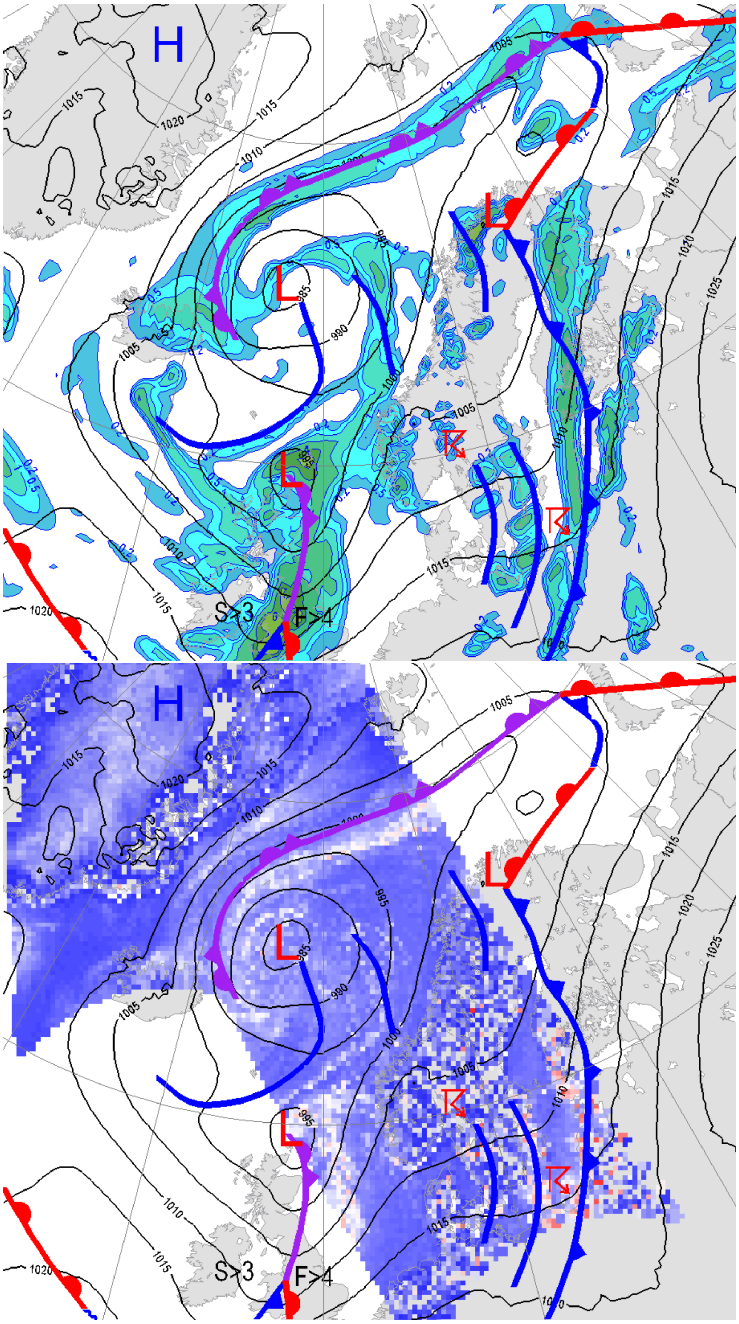

Figure F-11: *Weather situation on 28 September, 2005, 18UTC. Upper panel: HIRLAM pressure analysis, forecaster's analysis and a short range precipitation forecast. Lower panel: As above, but with R-factor imagery instead of precipitation forecast.*

and when the forward model is used in cloudy conditions, the RTTOV model error increases, and usually a bias error occurs.
In the experiments presented in this report there is no masking of AMSU-A observations that are contaminated by cloud water. Instead, the Norwegian Meteorological Institute has developed a theory for optimal asymmetric quality control. This approach is based on the Bayesian risk of assuming that the observation error has a normal distribution, when it actually has a non-normal distribution.

3.2.2 Developments in the project

Emissivities A natural basis for emissivity modelling would be to split the detected radiance into contributions from open water and various surface types in the footprint, assuming a constant surface temperature. If the surface is divided into three types, water with concentration c_W, first-year ice with concentration c_F and multiyear ice with concentration c_M, we can estimate the emissivity as a sum of the emissivities characteristic of the three types as

$$e = c_W e_W + c_F e_F + c_M e_M, \tag{13}$$

where we have $c_W + c_F + c_M = 1$.
This formulation is also used in the derivation of sea ice concentration algorithms such as for instance the NASA Team algorithm. We have estimates of the three concentrations from SSM/I data and can try to determine a typical emissivity for each of the three surface types for the desired AMSU microwave frequencies. If we do the assumption that the ice types distinguished from the SSM/I channels also are relevant for emissivity properties in the AMSU sounding channels, this gives a simple method for emissivity estimation.
An interface has been made to the Ocean and Sea Ice SAF (OSI-SAF) output which reads total and multiyear sea ice concentration data at the AMSU-A footprint in order to use that for emissivity estimation.
As a first test of the system we just input $e = 1$ over sea ice, and this has been used in the first assimilation experiment described here. Such an experiment is not so meaningful for testing the channels sensing the surface, but, as will be discussed below, can be used to assess the effect of assimilating the upper channels and to monitor the surface channels in passive mode.
The next step was to input realistic emissivities for first-year and multiyear ice using the OSI-SAF concentrations in the above formula. L. Toudal (pers. comm., project part 3) has provided AMSU emissivities from data from the Kara Sea (first-year ice) and from an area North of Greenland (multiyear ice). These data are given in Table T-3.
Figure F-12 shows the observed versus modelled brightness temperatures for the simple experiment using emissivity 1.0 and for the refined scheme using the OSI SAF concentrations with the emissivity values from Toudal as described above, for a surface channel, channel 2. Similar intercomparisons for channels getting information higher up in the atmosphere show that this formulation gives a better fit to the observations also for those channels.

Quality control Before assimilating data, a quality control is performed to reject observations which are contaminated by clouds in such a way that they are not well described by the forward model or contaminated with other types of gross errors. Such errors are generally non-Gaussian, and the observations would have a detrimental effect on the verification scores if used.
The observation quality control method used for the experiments presented in this report estimates the increment in the verification score when we assimilate each observation with non-normal error probability distribution while assuming that it has normal error distribution. If it is expected that the verification score will improve, the observation is used, otherwise it is discarded. The method is described in detail in Tveter [2005]. In short, the Bayesian risk is formulated so that it reflects the improvement in the impact which we

Table T-3: *Ice emissivity values for AMSU-A channels*

AMSU-A channel 1	Freq. [GHz]	Emissivity	
		First-Year ice	Multiyear ice
1	23.8	0.971	0.874
2	31.4	0.970	0.829
3	50.3	0.928	0.796
4	52.8	0.928	0.796
5	53.596	0.928	0.796
6	54.4	0.928	0.796
7	54.94	0.928	0.796
8	55.5	0.928	0.796
9–14[a]	57.290	0.928	0.796
15	89.0	0.913	0.744

[a]Channels 9 to 14 are clustered around 57.290 344 GHz, see the NOAA KLM Guide http://www2.ncdc.noaa.gov/docs/klm/html/c3/sec3-3.htm

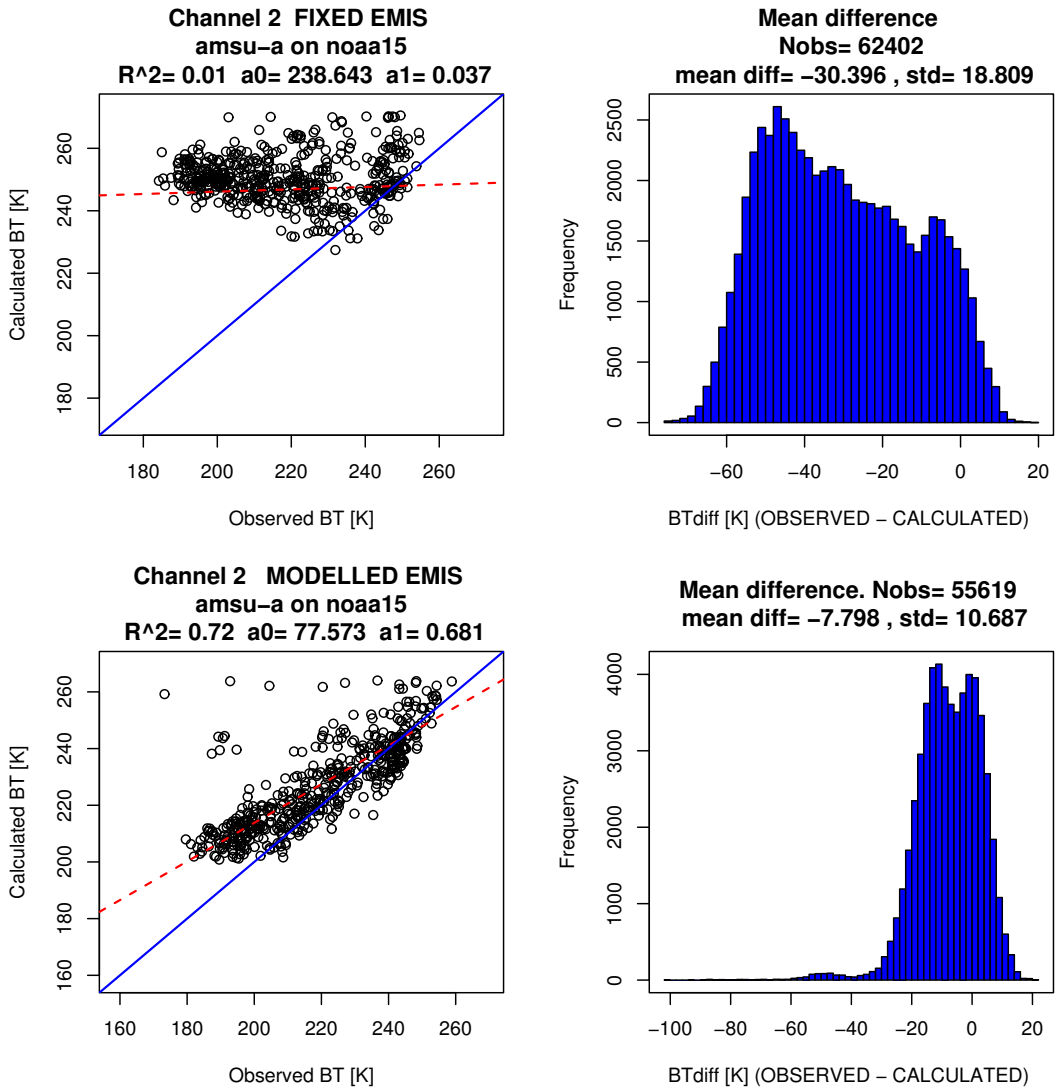

Figure F-12: *Scatterplot of observed versus modelled brightness temperatures and histogram for departures for AMSU channel 2: Top: with constant sea ice emissivity; bottom: with ice-type dependent emissivity estimated as described in the text.*

would have if we used an observation with non-normal error distribution, while the assimilation system assumes it has normal error distribution. The risk increment is given as a function of the innovation, i.e., the departure between the observation (Y) and the first guess equivalent (HX_b). If the risk increment is less than zero, the observation has a positive effect on the analysis (i.e., the mean squared error verification score will improve). The innovation thresholds for 'valid' AMSU-A observations are determined so that each accepted channel gives a negative risk increment.

3.2.3 Main results

General results To evaluate the implemented system, an impact study was set up with a "reference" and an "experiment". The reference was chosen to be fairly close to the operational met.no HIRLAM version, except it has no assimilation of satellite observations (operationally QuikScat ocean wind data and AMSU-A data over ocean are used). The experiment differs from the reference in one way, namely by assimilating AMSU-A data over sea ice. Differences between these two runs can therefore directly be attributed to assimilation of these observations. By not using satellite data over ocean in any of the runs, it is easier to discover any impact of using AMSU-A observation over sea ice.

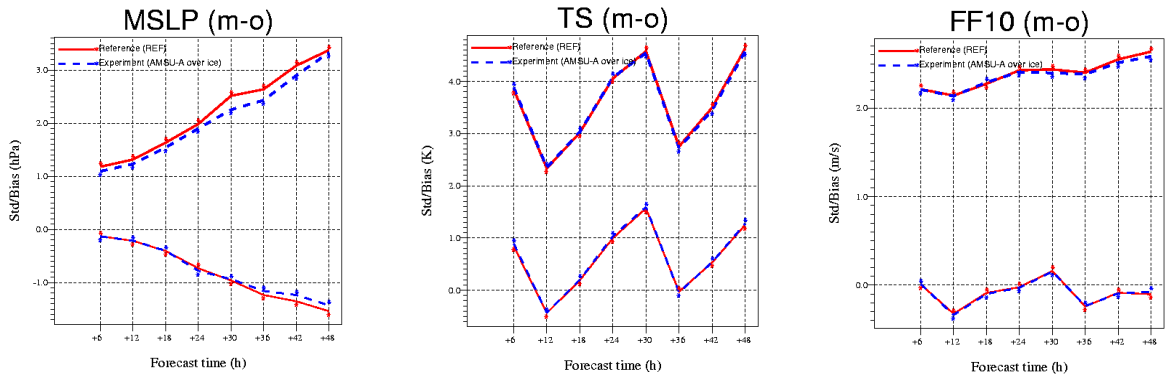

Figure F-13: *Error (difference between model and observation, m-o) of mean sea level pressure (MSLP, left), temperature at 2 m height (T2m, centre) and 10-m wind speed (FF10, right) as a function of forecast length, in the reference and experiment. Northern observations only. Red solid line: reference; blue dashed: experiment.*

In Figure F-13 we have verified the forecasts from the reference and experiment using a Northern observing station data set of conventional meteorological observations. Here we see some differences between the curves, particularly for the sea level pressure (MSLP), where the experiment scores improve for the period investigated.

A case study Monitoring the impact of the AMSU-A observations as a function of time, we find that it is variable, and there are periods and situations when the impact is particularly large. In Figure F-14 we present 24 hrs forecasts for a case with particularly large difference between the experiment and reference. The figure shows a small section of the total NWP model domain.
In general the two runs give very similar results away from the Arctic. However, there is a low pressure system in the Barents Sea between Norway and Spitsbergen which is different in shape, strength and position. There are significant differences in this area, elsewhere differences are smaller.
In this region there is a northerly flow (i.e., southwards) from the sea ice regions. The upper air charts show that over parts of the area such a flow extends to the mid and upper troposphere. This means that

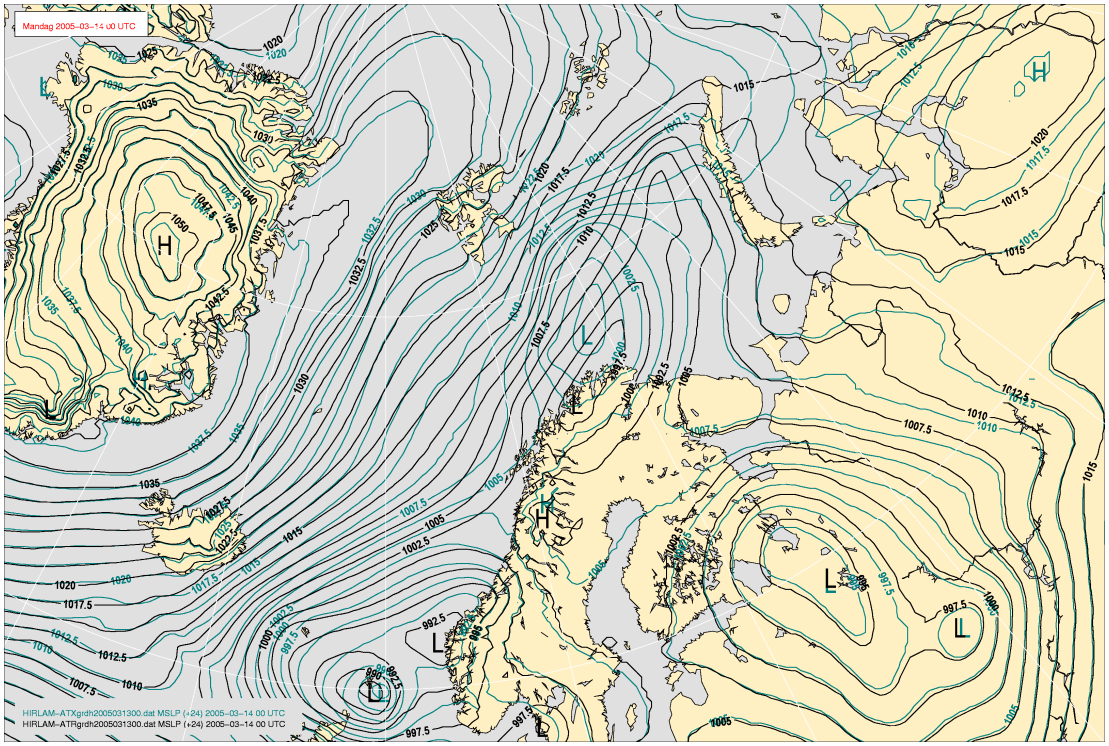

Figure F-14: *Weather situation on 14 March, 2005, 00UTC, 24 hrs forecast. Black: reference, green: experiment using AMSU-A over sea ice.*

influences of added observations above the sea ice can propagate southwards into the area where the large differences between reference and experiment are found.

For verifying which of the two forecasts is closest to reality, it is of interest to compare with model analyses over the area. Usually the differences between the analyses of the reference and experiment are much smaller than differences between forecasts from the reference and the experiment. In Figure F-15 we present analyses from the two cycles valid at the same time. We find surprisingly large differences between the two analyses, and observe that the differences between the two 24h forecasts are basically maintained in the analysis. There are areas where the difference between the two analyses is more than 10 hPa. The reason for this must be that there are very few conventional observations in the region which by assimilation can make the two cycles approach each other. There is almost no conventional observation in the Barents Sea where the two low pressure systems are located. There are quite a few observation stations on the coast of Northern Norway as well as in Spitsbergen, but in these areas there are not so large differences between the two cycles. These two different analyses can therefore not be used for verification.

To see which of the two cycles has the analyses (and forecasts) closest to reality, we remain with two island observations in the area, Bjørnøya and Hopen. An enlarged chart with some selected observations is shown in Figure F-16.

Bjørnøya is somewhat to the west of the low pressure centre. Even if the match of the indicated observed wind direction with the wind direction that corresponds to the isobars is not very good, neither with the reference nor with the experiment model, this station matches the analysis from the experiment run significantly better than the reference. The same is the case for the station at Hopen Island, just south of Spitsbergen.

In this situation impact of the added AMSU-A observations remains in the model for a long time and

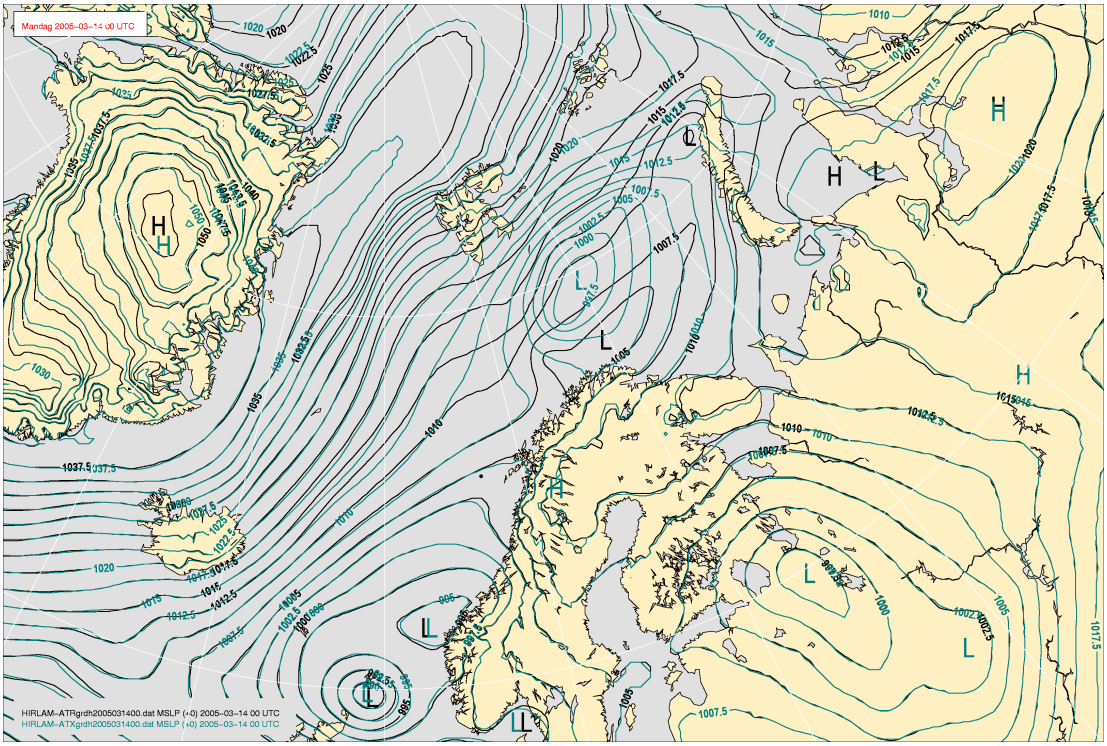

Figure F-15: *Weather situation 14 March 2005 00UTC, analysis. Black: reference, green: experiment using AMSU-A over sea ice.*

affects the simulated circulation pattern in the Barents sea. It seems that the added AMSU-A information over ice is clearly beneficial.

3.2.4 Conclusion, recommendations

AMSU-A observations over sea ice were successfully assimilated in HIRLAM 3D-Var at the Norwegian Meteorological Institute. A new approach for estimating microwave sounding channel emissivity over sea ice was developed using information from the EUMETSAT OSI SAF. A quality control method developed specifically to handle asymmetric (cloud water) contamination was also developed. Assimilating AMSU-A observations over sea ice using the proposed approach had a positive effect on the MSLP and temperature profiles, especially in northern areas.

It is generally difficult to measure the impact of the added observations over the sea ice regions, because there are almost no conventional observations which can be used for verification in the region. When we measure the impact using the conventional observation network over Europe, we find that the impact varies with circulation pattern, and that the largest positive impact coincided with general upper flow from the sea ice towards the North Atlantic. This clearly shows that there is information contained in these observations which the assimilation system can benefit from.

In particular we saw that in areas in the Barents sea with sparse conventional observation coverage, the positive impact could remain in the model for a long period of time, and that in the absence of satellite data, problems of rejection by quality control can occur. This shows the importance of adding new data in data sparse regions, but also the importance of increasing the robustness of the assimilation system by having a certain density of observation information to avoid data rejection problems.

Even if the experiment period is limited in time, and the positive impact seem to originate from a few

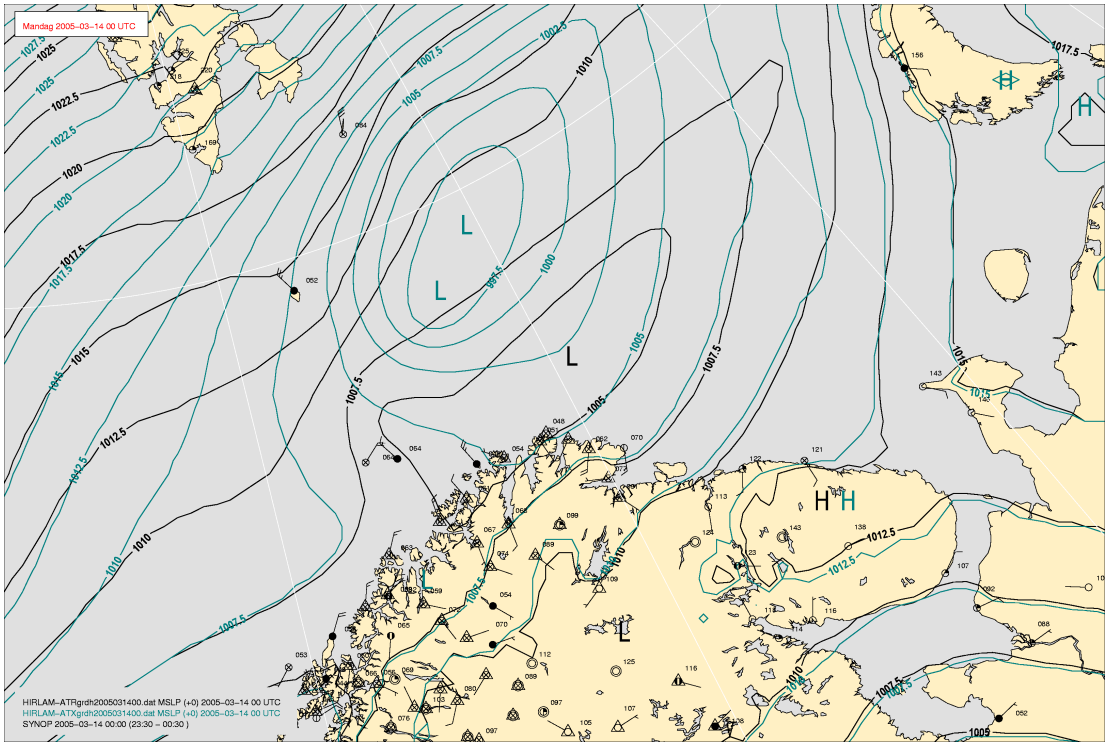

Figure F-16: *Weather situation 14 March 2005 00UTC, analysis and selected observations. Black: reference, green: experiment using AMSU-A over sea ice.*

incidents within this period, this study strongly indicates benefits of adding AMSU-A observations over sea ice, and it should be planned to include this in operational model runs with HIRLAM.

3.2.5 Use of AMSU-B and humidity data

The goal was to develop the analysis code HIRVDA (HIRLAM variational data assimilation) in the NWP system HIRLAM so that it could assimilate TWV retrievals and raw AMSU-B radiances over open sea as well as over sea ice. The outcome of the project is a system that can assimilate TWV retrievals over sea ice and raw AMSU-B radiances over sea in humid conditions.

3.2.6 Total water vapour retrievals

The retrievals were produced off line by the partner at the Danish Technical University (DTU) using the algorithm (developed by the partner at the University of Bremen) and transferred to SMHI by ftp. The reason why the retrievals are only useful over sea ice can be understood by looking at the difference between TWV retrievals and modelled TWV. Over ice this difference has a nice Gaussian distribution whereas over open sea it is clearly skewed towards negative values. The problem is that the method used in producing the retrievals only works when the atmosphere contains low amounts of water vapour, as is often the case over sea ice in the Arctic. At lower latitudes, where the sea is mostly open, there are often higher amounts of water vapour that will result in erroneous retrievals. This is not a problem since we can chose only to use the retrievals in situations with sea ice.
The results from the validation experiments using the TWV retrievals are promising but rather uncertain. The impact was studied in an experiment using data from all of January 2005. The HIRLAM model was run through the whole month two times. Once in a reference run, using only conventional observations

together with AMSU-A data over open sea and once with additional observations in terms of the TWV retrievals. Comparing the two model runs it can be noticed that the main changes in the model remained in the Arctic region. The conclusions, from looking at differences between the experiments and comparing against observations, were: The TWV retrievals increased the water vapour amount and cloudiness in the model. This, in turn, led to a warmer model which scored a bit better on temperature, MSLP (mean sea level pressure) and geopotential. However, it turned out that the errors in the 2 meter temperature where very high in the control run to begin with. Thanks to this observation, an error was discovered in the surface scheme ISBA (Interactions between Surface–Biosphere–Atmosphere) over ice. As a result of these experiments a correction was introduced into the SMHI operational suite that led to an immediate warming of several degrees in the Arctic. At this point it is therefore hard to say how valuable the TWV retrievals actually are to the model. In the validation experiment, they acted as a bias reducer for the model by providing more water vapour, clouds and therefore a warming, which was just what the model needed. It is, however, better to solve such problems by correcting the physics.

3.2.7 Raw AMSU-B radiances

Following the recommendation from User Advisory Group member Steven English (The Met Office, UK) we have focused on assimilation of raw radiances instead of TWV products. A data stream for the direct measurements of the AMSU-B radiances, redistributed by EUMETSAT via the EARS service (Eumetsat ATOVS Retransmission Service), was set up in the beginning of the project and is up and running.
In order to assimilate raw radiances over open sea and sea ice three major problems needed to be solved:

1. Observation operator development
2. Quality control (cloud contamination)
3. Bias correction

As a result of this project promising solutions to all of these problems have been presented. However, they have not yet been put together into a working assimilation system. So far the system can only assimilate AMSU-B radiances over open sea in humid conditions, i.e., in situations opposite the ones where assimilation of TWV retrievals is possible.
An observation operator for AMSU-B based on the RTTOV-7 radiative transfer model has been implemented into one version of the HIRVDA system. Another version of the system was developed to include the surface skin temperature and surface emissivity in the control vector used for minimisation. This is necessary in order to deal with dry situations where the characteristics of the ground affects the AMSU-B measurements. The idea is that a decent first guess of the surface parameters from the HIRLAM model will suffice to make the minimisation converge to a realistic minimum. Preliminary results are promising. However, work remains to merge these two HIRVDA versions into one that is capable of assimilating raw AMSU-B data over open sea as well as over sea ice in humid and dry conditions.
The second problem has to do with the fact that the treatment of clouds in the NWP and the radiation transfer models is too crude to be useful. The AMSU instrument, working in the microwave region, is rather insensitive to clouds but there are situations where clouds do affect the measurements. These cases must be identified and excluded from the assimilation in the quality control. Initially, the AAPP (ATOVS and AVHRR Processing Package) software package was used to filter out cloudy observations. The large AAPP package is however not suitable for implementation in the HIRLAM system and it does not work for observations over sea ice. Anyway a cloud-cleared data set for open sea was produced.
This data set was then used to solve another problem - that of bias correction. Raw satellite radiance measurements are often biased compared to the model. This bias must be removed in order to arrive at a successful minimisation in the assimilation process. A result from the project is that the same bias

correction procedure can be used for AMSU-B as is already done operationally for AMSU-A with one exception - the total integrated water vapour content is excluded from the list of predictors.
Parallel to this work a cloud mask was developed based on the NWC-SAF (SAF on Support to Nowcasting and Very Short Range Forecasting) cloud type product using data from the AVHRR instrument on the same platform as the AMSU instrument. This mask works both over open sea and over sea ice by discarding observations from regions with clouds of certain types depending on the AMSU-B channel. Even though the cloud type product is known to have problems during the polar winter it seems that the quality is good enough for the crude screening needed to filter out the contaminated AMSU-B measurements. However, no validation studies have been made based on raw radiances, neither filtered by the AAPP package nor by the cloud mask developed within this project.

3.2.8 Surface heat flux

Early on in the project, another data stream was set up for the OSI SAF ice concentration measurements. The surface analysis in HIRLAM was then developed to produce and assimilate pseudo observations of these ice concentration measurements on the HIRLAM scale.
Practically oriented flux-calculation techniques based on correction functions to the neutral drag and heat/mass transfer coefficients have been further developed. In the traditional formulation, the correction functions depend only on the bulk Richardson number. However, data from measurements of turbulent fluxes and mean profiles in stable stratification over different sites[2] exhibit too strong variability in this type of dependencies. Indirect evidence from climate and weather prediction modelling also suggests that the traditional flux calculation technique is not sufficiently advanced: Comparing observed and modelled fluxes, observed data points are widely spread around modelled curves. It is thus conceivable that other mechanisms besides the surface-layer stratification and, therefore, other arguments besides the bulk Richardson number must be considered.
The proposed technique accounts for a difference between the roughness lengths for momentum and scalars and includes a new effect of the static stability in the free atmosphere on the surface layer scaling. Recommended correction functions depend, besides bulk Richardson number, on one more stability parameter, involving the Brunt-Väisälä frequency in the free atmosphere, and on the roughness lengths.
The project has resulted in an improved surface flux treatment and a new surface scheme using OSI-SAF ice concentrations implemented in HIRLAM. An experimental run has been done for January 2005 (120 forecasts, +48 hours each). The results were positive, there was significant improvement for the bias and the root mean square of mean sea level pressure, temperature at 2 meters, and humidity at 2 meters.

3.2.9 Conclusion

The objective of this project was not to bring the NWP developments into operational application. However, the bug in the HIRLAM system that was discovered thanks to the validation of the TWV retrievals led to a correction in the operational system that reduced the bias in the 2 m temperature in the Arctic region by several degrees. Also, the project results concerning developments in NWP humidity analysis and surface flux modelling are promising.
The results from the validation of assimilation of TWV retrievals from AMSU-B show that the induced model changes remained in the Arctic region and mainly resulted in increased water vapour amount and cloudiness. This, in turn, led to a warmer model which produced better forecasts on temperature, MSLP and geopotential.

[2] over sea ice: observations from SHEBA (Surface Heat Budget of the Arctic Ocean) and BASE (Beaufort Arctic Storms Experiment); over snow: observations from Antarctic station Halley (UK) and station Sodankylä (polar Finland)

The work on assimilation of raw AMSU-B radiances almost resulted in a working HIRVDA version. All the necessary parts are there but not in place. The cloud mask based on AVHRR data from the NWC-SAF cloud type product used within the OSI-SAF seems to be able to filter out observations that are contaminated by clouds both over open sea and over sea ice. However, the code is still in research mode and not integrated in the HIRVDA system. The HIRVDA system has been extended in two versions - one that is able to process the raw radiances and one that is able to include surface skin temperature and surface emissivity in the control vector during the minimisation. However, these two versions were not merged into a system that can handle cases with the typically dry Arctic atmospheres when the surface conditions become important for the assimilation. The reason why this happened is that the HIRVDA system is maintained in a variety of versions on a variety of platforms. The person responsible for the minimisation development was comfortable with one set up and the person doing the work on AMSU-B on another. Our idea was that the fastest route would be to make separate developments and then merge the result. If we had aimed at a uniform set up from the beginning, the software would be ready to use once developed. On the other hand, we still think that this approach would have taken at least the same amount of time as the one we chose to pursuit.

The development of a new surface heat flux scheme lead to a significant improvement in forecasts of the potential temperature at lower model levels in the cases of moderate and very stable stratification in comparison with the conventional technique. There was also improvement for the vertical profile of wind in the boundary layer. Verification scores obtained by forecasts with the new parameterisation of the surface fluxes against observations demonstrate a significant improvement in comparison with the current (reference) parameterisation for 2 meter temperature and humidity and for mean sea level pressure.

All in all, these developments should, if used operationally, result in greater confidence in short and medium term weather predictions which benefits the entire population of the Arctic region, the environment through improved risk management possibilities and better disaster control. Reliable forecasts are the first step in risk management and disaster control whether in the marine environment, the atmosphere or on land, and all economic activities and developments.

3.3 Part 3: Empirical model for emissivity and backscatter of sea ice

The purpose of this project part was to establish a set of baseline emissivity values of various sea ice types in order to improve ice concentration retrievals as well as atmospheric retrievals over ice.

The task was solved in two ways.

1. Empirical emissivities were derived from areas of known ice composition using microwave radiometer data from the AMSR-E and AMSU instruments.
2. A sea ice and snow emissivity model was developed and used in the evaluation and understanding of the empirically derived emissivities from 1.

3.3.1 Empirical determination of emissivities:

AMSR-E forward model of ice seen through the atmosphere: Radiative transfer theory provides the relationship between the observed brightness temperatures T_b [K] and some geophysical parameters. A model describing this relationship is known as a forward model, and here a forward model described by Wentz and Meissner [2002] has been used. The model describes the connection between 4 geophysical parameters (wind, water vapour, liquid water and sea surface temperature) and the brightness temperatures measured by AMSR. The model described by Wentz and Meissner [2002] is only valid for water surfaces, so the model has to be expanded to take ice-covered surfaces into account.

Inclusion of ice in the Forward Model In the ocean/atmosphere radiative transfer model by Wentz and Meissner [2002] the upwelling brightness temperature at the top of the atmosphere - the brightness temperature measured by the AMSR instrument - is written as:

$$T_{B\uparrow} = T_{bU} + \tau\,[eT_S + T_{b\Omega}] \tag{14}$$

where T_{BU} is the contribution of the upwelling atmospheric emission, τ is the total transmittance from the surface to the top of the atmosphere, e is the Earth surface emissivity and $T_{b\Omega}$ is the surface scattering integral.
A change in the surface content from open water to ice only has an influence on the following parts of the model: eT_S (the brightness temperature close to the sea surface) and $T_{b\Omega}$.
In order to be able to include ice in the model for the brightness temperature close to the sea surface, one has to consider the difference between the emissivity of an open water sea surface and an ice-covered sea surface.
The brightness temperature, $T_{b,ice}$, at the ice surface can be written as:

$$T_{B,ice} = T_{P,ice}e_{ice} \tag{15}$$

where $T_{P,ice}$ is the physical temperature of the ice surface and e_{ice} is the emissivity of the ice surface.
The emissivity of an ice covered surface depends on the type of ice cover, the polarisation and the frequency. The sea ice emissivities used to calculate the brightness temperatures of the different channels of the AMSR are given in the Tables T-4 and T-5. Table T-4 gives typical values for the autumn of 2003 (September-November) and Table T-5 gives values for the winter 2003/2004 (November-April).

Table T-4: *Emissivities at AMSR frequencies for first-year (FY) and multiyear (MY) ice used in the forward model (autumn 2003). "Vertical" and "Horizontal" refer to the polarisation.*

	Frequency	6 GHz	10 GHz	18 GHz	23 GHz	37 GHz
FY	Vertical	0.9204	0.9127	0.9373	0.9409	0.9347
	Horizontal	0.7502	0.7738	0.8314	0.8490	0.8600
MY	Vertical	0.9692	0.9284	0.8843	0.8554	0.7813
	Horizontal	0.8651	0.8356	0.7917	0.7792	0.7248

Table T-5: *Emissivities at AMSR frequencies for the first-year (FY) and multiyear (MY) ice used in the forward model (winter 2003/2004)."Vertical" and "Horizontal" refer to the polarisation.*

	Frequency	6 GHz	10 GHz	18 GHz	23 GHz	37 GHz
FY	Vertical	0.9905	0.9718	0.9817	0.9773	0.9567
	Horizontal	0.9097	0.9007	0.9072	0.9075	0.8927
MY	Vertical	0.9870	0.9487	0.8933	0.8494	0.7473
	Horizontal	0.8866	0.8627	0.8163	0.7871	0.7011

Now, the brightness temperature close to a surface mixed of open water, first-year (FY) and multiyear (MY) ice can be written as:

$$T_{B,S} = eT_S = C_{ow}T_{B,ow} + C_{FY}T_{B,FY} + C_{MY}T_{B,MY} \tag{16}$$

where C_{ow}, C_{FY} and C_{MY} and are the concentrations (= surface fractions) of open water, first-year and multiyear sea ice, respectively, and $T_{B,ow}$, $T_{B,FY}$ and $T_{B,MY}$ are the respective brightness temperatures of the three different surface types.

The surface scattering integral is given by Wentz and Meissner [2002], equation (61) as:

$$T_{B\Omega} = [(1+\Omega)(1-\tau)(T_D - T_C) + T_C]R \tag{17}$$

where T_D is the downwelling brightness Temperature, T_C is the cosmic background, and Ω is a fit parameter. In this equation it is only the sea-surface reflectivity, R, which is influenced by the ice. An effective reflectivity for a mixed surface can be written as:

$$R_{eff,mix} = 1 - e_{eff,mix} = 1 - (C_{ow}e_{ow} + C_{FY}e_{FY} + C_{MY}e_{MY}) \tag{18}$$

where C_{ow}, C_{FY} and C_{MY} are the concentrations of the three surface types and e_{ow}, e_{FY} and e_{MY} are the emissivities of the surface types.
The last thing one has to take in to consideration when including ice in the model is that the forward model described by Wentz and Meissner [2002] has a surface temperature included. This temperature has to take the temperature of the ice into account and therefore the surface temperature used in the ice model has to be calculated by:

$$T_{S,mix} = C_{ow}T_{P,ow} + C_{ice}T_{P,ice} \tag{19}$$

where C_{ow} and C_{ice} are the concentrations of open water and sea ice, respectively, and $T_{P,ow}$ and $T_{P,ice}$ are the respective physical surface temperatures. This mixed surface temperature only has to be used in the part of the model concerning the atmosphere, not in the parts concerning the dielectric constant of sea-water and the wind-roughened sea surface.

Empirically derived AMSU-A and B emissivities of FY and MY ice: The radiative transfer equation for the total microwave radiation received at satellite altitude can be written as:

$$T_b = eT_s(1-a) + aT_a + aT_a(1-a)(1-e) + T_{sp}(1-a)^2(1-e) \tag{20}$$

where:

T_b is the microwave brightness temperature
T_s is the temperature of the surface (the emissive layer)
a is the absorption coefficient for the atmosphere
T_{sp} is the brightness temperature of space (2.7 K, “cosmic background”)
e is the emissivity of the surface (the one we want to find from T_b measurements)
T_a is the temperature of the atmosphere

The basic idea is that the downwelling atmospheric brightness temperature (T_{dn}) can be estimated/modelled using an atmospheric radiative transfer model (MWMOD). This allows us to calculate the total atmospheric absorption coefficient at each of the AMSU frequencies.

$$T_{dn} = T_{sp}(1-a)T_a \tag{21}$$

Solving for a yields

$$a = \frac{T_{dn} - T_{sp}}{T_a - T_{sp}} \tag{22}$$

Inserting this in the basic radiative transfer equation (20), we can now solve for e:

$$e = \frac{T_b - aT_a - (1-a)aT_a - T_{sp}(1-a)^2}{T_s(1-a) - a(1-a)T_a - T_{sp}(1-a)^2} \tag{23}$$

which allows us to estimate e from measurements of T_b.
The assumptions are that the atmospheric attenuation can be reasonably approximated by absorption coefficient and reference temperature, and in the following application we will assume a minimal water vapour load so the main contribution to the absorption is from oxygen.
The plot below (Figure F-17) shows the atmospheric absorption at the AMSU frequencies as modelled using the MWMOD model.

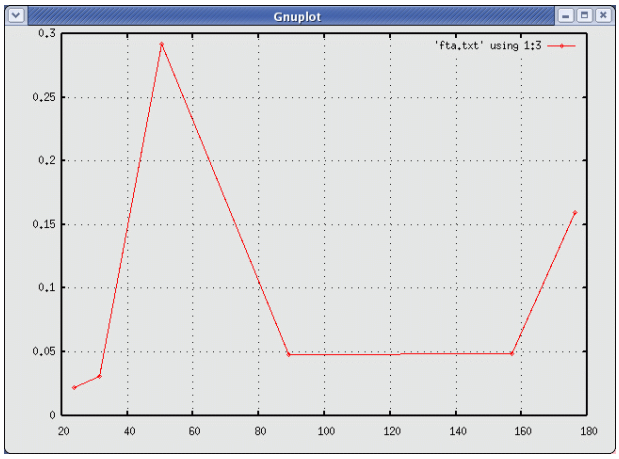

Figure F-17: *Atmospheric absorption coefficient at AMSU frequencies assuming a minimal water vapour load.*

The calculated downwelling temperatures are given in Table T-6:

Table T-6: *Downwelling brightness temperature T_{dn} at each AMSU frequency band*

Frequency [GHz]	T_{dn} [K]
23.8	8.2
31.4	10.4
50.3	76.4
89.0	14.8
150.0	15.0
176.3	43.0

Results: Figure F-19 shows the derived emissivities from the FY ice area, and Tables T-7 and T-8 (centre column) summarise the results in a form suitable for input to the atmospheric data assimilation in project part 2.
Figure F-20 shows the derived emissivities from the MY ice area, and Tables T-7 and T-8 (rightmost column) summarise the results in a form suitable for input to the atmospheric data assimilation in project part 2. A software package implementing the derived emissivities was delivered to project part 2.

3.3.2 Microphysical model of ice and snow emissivities:

Introduction The strategic importance of sea ice emission models is to relate physical properties of the target to brightness temperatures (T_b) at different microwave frequencies (ν) and polarisations and further to interpolate between observations at different places and frequencies. Because the radiance received at the satellite generally contains contributions from both atmosphere and surface, the surface

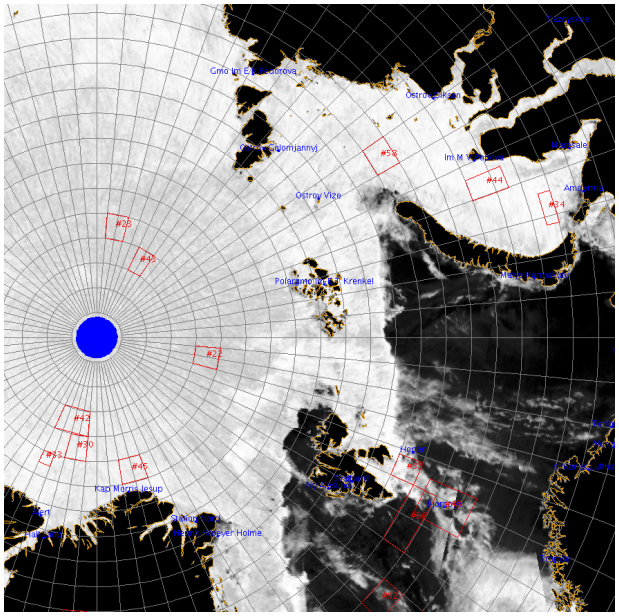

Figure F-18: *Map of part of the Arctic Ocean showing the location of the first-year-ice study area (58) in the Kara Sea and the multiyear-ice study area North of Greenland (45). The locations used in the present study are subsections of areas 45 and 58. The purple arrows point at the locations of the meteorological stations that provided the air temperatures used as T_a. Specification of areas: First-year ice: Kara Sea (76.5-77°N, 77–79°E) and multiyear ice: N. Greenland: (84–84.6°N, 32–35°W)*

emission model relationships are needed for the retrieval of both surface and atmospheric parameters. While there are physical microwave models describing the atmosphere, the open ocean and partly the land covering a wide range of microwave frequencies and polarisations, such models are generally missing for ice-covered polar regions. The importance of sea ice emission models is illustrated in the applications of this chapter. The aim here is to give a short overview over the quantitative influence of different microphysical parameters in sea ice and the snow on top of it at 50° incidence angle and how these link to emissivity, brightness temperature, dielectric properties and scattering exemplified by using a sea ice version of the Microwave Emission Model for Layered Snow-packs (MEMLS). We further present two examples of sea ice emissivity modelling applications: sensitivity of emissivity to snow parameters at sounding frequencies and sea ice concentration estimate sensitivity to ice surface emissivity. For a more in depth treatment of the sea ice emissivity model and additional examples, the reader is referred to Tonboe et al. [2005]. Within IOMASA, there were three sea ice emissivity modelling applications: sensitivity of emissivity to snow parameters at sounding frequencies, sea ice concentration estimate sensitivity to ice surface emissivity, and investigation of the potential of new sensors (i.e., ESA's Soil Moisture and Ocean Salinity, SMOS) for sea ice mapping.

Sea ice emission modelling The permittivity (ε) of snow is determined by its density and liquid water content [Ulaby et al., 1986]. The permittivity of snow affects the reflection, transmission and the absorption coefficients. Scattering in the snow pack is detectable for frequencies higher than 10 GHz [Barber et al., 1998] and is important for coarse snow grains or high frequency (>20 GHz) [Mätzler, 1987]. The permittivity of sea ice is largely given by the brine and air-inclusion volume [Shokr, 1998]. Important for scattering in sea ice is the size and number density of brine pockets or air bubbles [Winebrenner et al., 1992].

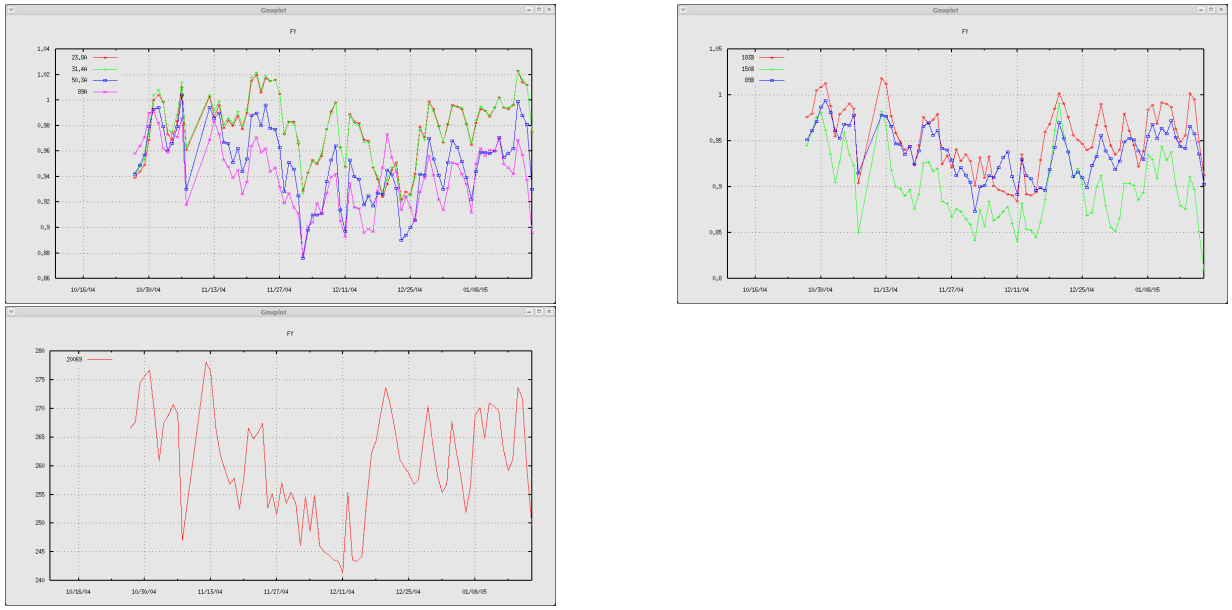

Figure F-19: *Empirically derived emissivities of first-year ice at AMSU-A frequencies (upper left), AMSU-B (upper right) and time series of surface temperatures for reference (lower left)*

Important radiative processes in a homogeneous snow cover can be described using simple emission models [Ulaby and Stilles, 1980; Mätzler, 1987]. However, snow cover on land, ice or sea ice is a layered medium and therefore the simple models fail to simulate observations by not accounting for important reflections between layers [Mätzler et al., 1984; Surdyk and Fily, 1993]. Winebrenner et al. [1992] provide a review of different types of emission models that exist for sea ice. The Microwave Emission Model for Layered Snow-packs (MEMLS) is a "model suitable for simulations of all kinds of physical effects" [Mätzler et al., 2000, p. 107] and it has been tested and validated for snow-cover on land with satisfactory results. Here MEMLS is extended to include emission from sea ice. The sea ice model and modifications are described in the next section.

Extension of MEMLS to sea ice emission MEMLS, described in Wiesmann and Mätzler [1999], uses the physical snow quantities and structure as input, i.e., sequence of layers (j), density (ρ), exponential correlation length (p_{ec}), thermometric temperature (T) and moisture (W). In order to apply this model to compute the emission of both snow and sea ice it is necessary to include modules that compute the dielectric properties, and scattering of sea ice. Small liquid brine inclusions also called brine pockets dominate scattering in nilas and first-year ice. In multiyear ice, the voids and air bubbles in the upper ice are the primary scatterers [Nghiem et al., 1995]. The permittivity of liquid brine is an order of magnitude larger than the permittivity of solid ice and the permittivity of sea ice is therefore primarily a function of brine volume [Ulaby et al., 1986].
The permittivity of sea ice is computed using Polder - Van Santen mixing formulas described in, e.g., Shokr [1998]. It is a function of pure ice permittivity, inclusion shape and orientation, volume and the brine pockets' permittivity (spheres are used because sea ice is assumed isotropic here). These mixing formulas do not account for scattering and therefore the accuracy of the permittivity estimates decreases as a function of frequency. Radiative processes at high frequency are usually confined to the snow cover and it is therefore not expected to be a significant source of error.
MEMLS is valid for snow cover in the range 5-100 GHz. The primary limitation is the estimation of

Table T-7: *Summary of derived sea ice emissivities at AMSU-A frequencies*

AMSU-A channel l	Freq. [GHz]	Emissivity	
		First-Year ice	Multiyear ice
1	23.8	0.971	0.874
2	31.4	0.970	0.829
3	50.3	0.928	0.796
4	52.8	0.928	0.796
5	53.596	0.928	0.796
6	54.4	0.928	0.796
7	54.94	0.928	0.796
8	55.5	0.928	0.796
9–14[a]	57.290	0.928	0.796
15	89.0	0.913	0.744

[a]Channels 9 to 14 are clustered around 57.290 344 GHz, see the NOAA KLM Guide http://www2.ncdc.noaa.gov/docs/klm/html/c3/sec3-3.htm

Table T-8: *Summary of derived sea ice emissivities at AMSU-B frequencies.*

AMSU-A channel l	Freq. [GHz]	Emissivity	
		First-Year ice	Multiyear ice
16	89.0	0.913	0.744
17	150.0	0.864	0.756
18	183.31±1	0.911	0.863
19	183.31±3	0.911	0.863
20	183.31±7	0.911	0.863

the scattering coefficient using empirical relations, which fit scattering in natural snow cover. For use of MEMLS outside of this frequency range, and for sea ice, it is necessary to compute the scattering coefficient using theoretical relations [Mätzler and Wiesmann, 1999].

The scattering in sea ice is therefore computed using the improved Born approximation (Mätzler, 1998). "The scattering [using the improved Born approximation] increases by a power law of the microwave frequency times the correlation length with a power of approximately 2.5. Above a certain frequency or above a certain correlation length, the increase will saturate in a similar way as Mie scattering does for spheres." [Mätzler and Wiesmann, 1999, p. 317]. It is further noted by Mätzler and Wiesmann [1999] that the improved Born approximation fits observations for snow grains which are large compared to the wavelength. It is therefore assumed, in this study, that the improved Born approximation is valid also at high frequency (157 and 183 GHz). Scatterers are exclusively air bubbles and voids in multiyear ice and brine pockets in first-year ice. The scattering coefficient is in general a function of the permittivity of pure ice, the permittivity of brine or air, the permittivity of the sea ice mixture, volume of brine or air, microwave frequency and the correlation length of scatterers. The exponential correlation length (p_{ec}) is a measure of scatterer size and distribution, see, e.g., Mätzler [2002].

Natural snow cover consists of both rounded and oblate grains. Re-crystallised snow grains have cup-like forms [Mätzler, 2002]. Congelation first-year ice has vertically oriented needle shaped brine pockets while frazil first-year ice has randomly oriented elongated brine pockets [Shokr, 1998]. The upper centimetres of first-year ice typically consist of frazil and deeper ice of congelation ice. Frazil layers may also appear at depth [Weeks and Ackley, 1986]. In this study both, the snow and sea ice scattering and dielectric prop-

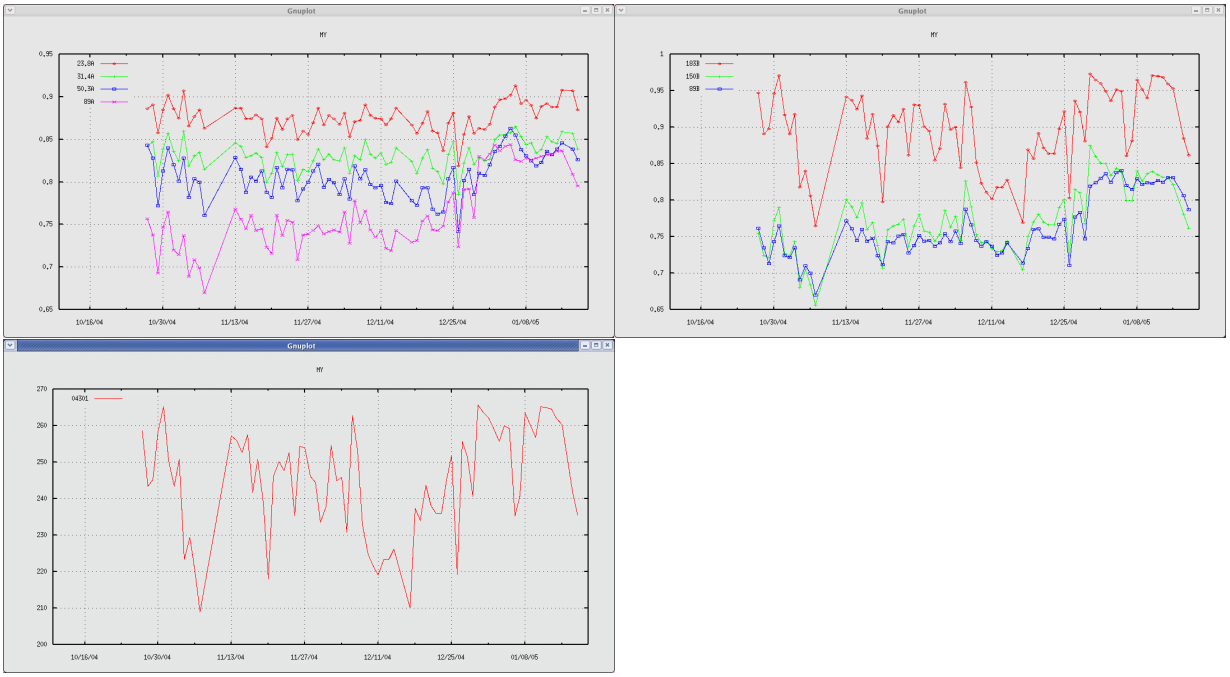

Figure F-20: *Empirically derived emissivities of multiyear ice at AMSU-A frequencies (upper left), AMSU-B (upper right) and time series of surface temperatures for reference (lower left)*

erties are assumed isotropic. This assumption significantly simplifies the a priori input to the model and the interpretation of the results, although it is in conflict with the description of the special types of snow and ice above. Anisotropy is a secondary effect that should be included in case specific studies, however, here we are interested in the primary properties affecting the emissivity in a more general description. These additional modules (sea ice scattering and dielectrics) are hence included in the model computation scheme. The MEMLS code is in MATLAB. With a few minor changes, this sea ice version of MEMLS is now running in GNU Octave, a free MATLAB clone (www.octave.org). For a more in depth treatment of the sea ice emissivity model and additional examples, the reader is referred to Tonboe et al. [2005].

Sea ice emission modelling experiments using MEMLS

The sea ice profiles: First-year and multiyear ice The constructed profiles of first-year ice and multiyear ice with typical properties for these ice types are used as input to the model. Tables T-9 and T-10 present the input parameters. For both profiles the skin temperature (synonymous with the upper 1 cm) is -15°C (258.15 K). The ice/ water interface temperature is -1.8°C (271.35 K). The temperature profile (1 cm increments) in snow and ice is linear with thermal conductivity in the snow and ice of 0.3 W/mK and 2.1 W/mK, respectively. During simulations with liquid water in the snow, the snow temperature is constant -1°C and the snow/ice interface temperature is -5°C. The multiyear ice profile is adapted from Mätzler et al. [1984] and the first-year ice profile is constructed to fit satellite T_b measurements [Tonboe and Andersen, 2004].

Parameterisation of sea ice emissivity for atmospheric retrieval The assimilation of atmospheric parameters derived from microwave satellite data, e.g., AMSU has a significant impact on both global

Table T-9: *First-year ice profile used as input to MEMLS. The permittivity, ε, of the sea ice is frequency dependent. Permittivity at frequencies 1.4, 37 and 183 GHz cover the range for both the permittivity real part and the loss factor. The permittivity, ε, at these frequencies is indicated by the superscripts: a: ε at 1.4 GHz, b: ε at 37 GHz and c: ε at 183 GHz.*

No. j	Layer depth z_j [m]	Density ρ [kg/m^3]	Exponential correl. length p_{ec} [mm]	Salinity S [psu]	Permittivity ε
1	0.00	260	0.07	0	1.43+0.00i
2	0.07	410	0.10	0	1.76+0.00i
3	0.12	300	0.14	0	1.56+0.00i
4	0.13-1.15	920	0.15	7	3.62+0.04i^a 3.45+0.17i^b 3.26+0.09i^c

(ECMWF) and regional (HIRLAM) weather prediction models [Prigent et al., 2004]. The principle is to separate the atmospheric emissivity from the surface emissivity in the T_b measurements from space, thus the atmospheric part is parameterised in terms of temperature or water vapour. The surface emissivity, which is high for sea ice compared to open water, can be determined at frequencies where the atmosphere is largely transparent in the 'atmospheric windows'. This allows referring the emissivities at the sounding frequencies to those at the window frequencies by interpolation using emission models. Temperature sounding uses frequencies around 50 GHz and humidity sounding uses frequency 85 GHz. Surface emissivity estimation at sounding frequencies will become even more important with SSM/IS because it combines observations at the window and at the sounding frequencies on one sensor observing at all frequencies with a constant incidence angle.

Figure F-21 shows the simulated correlation between first- and multiyear ice T_v at the 10 microwave frequencies (1.4-183 GHz) using all parameter pairs described in Table T-11 (T_v is the brightness temperature measured at vertical polarisation). The many off-diagonal points at the 37/50 GHz (Figure F-21f), 50/89 GHz (Figure F-21g) and 89/157 GHz (Figure F-21h) plots indicate that simple linear models are inadequate to relate T_v at window frequencies to sounding frequencies.

The nilas T_v is lower at the lowest of the two frequencies in each of Figure F-21a–e (frequency 37 GHz). The nilas points follow a line-like cluster about 45° to the diagonal. For higher frequency, the nilas points are close to the diagonal. The snow thickness/ snow liquid water parameter pair T_v points are close to the diagonal except in Figure F-21h where T_v (157 GHz) is lower than T_v (89 GHz). In Figures F-21f–i the off-diagonal points are associated with the upper snow density/bottom snow layer correlation length parameter pair for both first-year and multiyear ice. This is the most important parameter combination among the pairs in Table T-11 for the first-year and multiyear ice T_v sensitivity at medium and high frequency. The T_v variability is similar when varying more than two parameters simultaneously, e.g., first-year ice upper and mid snow density, bottom snow correlation length and salinity (not shown).

3.3.3 Conclusions

An empirical emissivity model has been established for both the AMSR-E microwave frequencies in the range from 6.9 to 89 GHz, and for the AMSU frequencies (23-183 GHz). The AMSU model has been implemented as a software module and integrated into the data assimilation scheme of met.no (project part 2) and the AMSR-E model has been used in a long term validation experiment in an optimal estimation algorithm at DTU (see project part 5). A microphysical emissivity and backscatter model has been implemented in collaboration with DMI, and used in an extensive evaluation of sea ice concentration

Table T-10: *Multiyear ice profile used as input to MEMLS. The permittivity, ε, of the sea ice is frequency dependent. Permittivity at frequencies 1.4, 37 and 183 GHz cover the range for both the permittivity real part and the loss factor. The permittivity, ε, at these frequencies is indicated by the superscripts: a: ε at 1.4 GHz, b: ε at 37 GHz and c: ε at 183 GHz.*

No. j	Layer depth z_j [m]	Density ρ [kg/m^3]	Exponential correl. length p_{ec} [mm]	Salinity S [psu]	Permittivity ε
1	0.0	260	0.07	0	1.43+0.00i
2	0.07	450	0.10	0	1.85+0.00i
3	0.08	300	0.10	0	1.52+0.00i
4	0.10	450	0.10	0	1.85+0.00i
5	0.11	300	0.10	0	1.52+0.00i
6	0.16	450	0.10	0	1.85+0.00i
7	0.17	300	0.14	0	1.52+0.00i
8	0.19	750	0.25	0.5	3.20+0.00i^a 3.20+0.01i^b 3.18+0.01i^c
9	0.29-2.49	900	0.20	2.5	3.31+0.01i^a 3.26+0.05i^b 3.21+0.03i^c

algorithms (project part 4) as well as in an assessment of the most important snow parameters influencing the emissivity of the ice/snow surface (see above).

Table T-11: *The parameters which are varied in sensitivity studies (p_{ec} is the exponential correlation length).*

Ice type	Parameter	Depth [cm]	Range
Nilas/young ice	Salinity	entire ice column	2.5-18 ppt
	Ice thickness	-	3-31.5 cm
First-year ice	Upper snow density	0-7	260-450 kg/m^3
	Mid snow density	7-12	260-450 kg/m^3
	Bottom snow p_{ec}	12-13	0.07-0.45 mm
	Upper ice salinity	13-19	2.5-18 ppt
	Snow liquid water	entire snow column	0-14%
	Snow thickness	-	1.5-31.5 cm
Multiyear ice	Upper snow density	0-4	260-450 kg/m^3
	Mid snow density	4-17	260-450 kg/m^3
	Bottom snow p_{ec}	17-19	0.07-0.45 mm
	Upper ice density	19-29	750-900 kg/m^3
	Snow liquid water	entire snow column	0-14%
	Snow thickness	-	1.5-31.5 cm

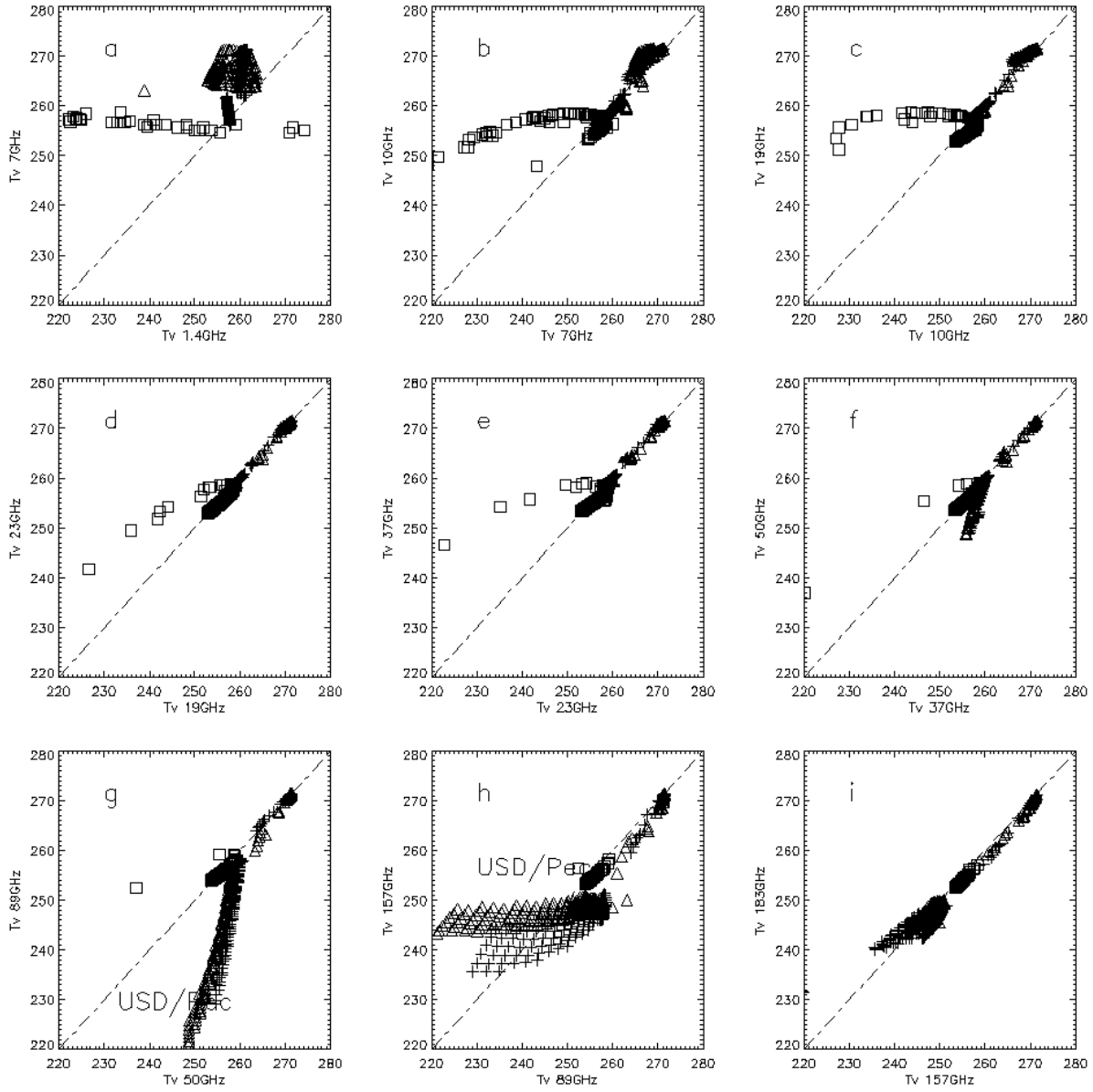

Figure F-21: *The simulated correlation between nilas (□), first-year ice (+), and multiyear ice (△) T_v for the 10 frequencies using all parameter pairs in Table T-11 (every 3rd data point). The off-diagonal points marked by USD/p_{ec} in plot g and h are associated with the upper snow density (USD)/ bottom snow layer correlation length (p_{ec}) parameter pair. The nilas T_v extends beyond the range of plots a–e.*

3.4 Part 4: Sea ice concentration retrieval

In the following we give results from emissivity modelling applied to atmospheric retrievals and retrieval of sea ice concentration as well as a summary of ice concentration algorithm intercomparisons against reference data from classified SAR (synthetic aperture radar) images, ice dynamics and ship observations. These sections are mostly a digest version of the literature produced in the project.

3.4.1 Introduction to emissivity modelling

The importance of sea ice emission models has been outlined above (section 3.3.2, p. 31).

Sea ice microwave emission measurements Formation environment, ice cover distribution, snow cover, ice surface roughness, ice density, ice salinity and air and brine inclusion content are important properties for the understanding and interpretation of sea ice microwave data. Emission models provide a link between these physical properties and microwave measurements and thereby to the understanding of measurements. Measurements are acquired from surface-based installations, aircraft or satellite. Polar orbiting satellites carrying microwave radiometers cover the globe daily with measurements and, in particular, cover polar regions several times a day. Reported sea ice measurements at different microwave frequencies cover the range from 1.4 to 183 GHz. For example, aircraft 1.4 GHz (L-band) measurements acquired recently over sea ice during summer melt [Klein et al., 2004]. Eppler et al. [1992, and the references herein], describe measured sea ice emissivities at frequencies between 4.9 and 94 GHz for different ice types. Hewison and English [1999] and Selbach [2003] report millimetre wavelength measurements between 89 and 183 GHz in the Baltic Sea and Arctic Ocean, respectively. Our focus is on the frequencies of 1.4, 7, 10, 19, 23, 37, 50, 89, 157, 183 GHz, which correspond to channels on present and future satellite sensors (e.g., CMIS, SMOS, SSM/I, AMSR, AMSU-B). The brightness temperature measured at these frequencies has different sensitivity to natural variability of snow and sea ice microphysical properties. The general appearance of the three predominant ice types in the Arctic, new-ice, first- year ice (FYI) and multiyear ice (MYI) is distinguishable using microwave remote sensing because of differences in dielectric and scattering properties. It is therefore convenient in this investigation to distinguish between these three major classes of sea ice.

Thin ice represented in the following by *nilas* belongs to the category new ice (thinner than 10 cm). It forms under quiescent conditions. It has a smooth surface with no or little snow cover and relatively high salinity, S, of 14-16 ppt. The density is about 920 kg/m^3 [Tucker et al., 1991]. Under continued growth, nilas will become young ice and eventually first-year ice.

The level *first-year ice* (0.3-2 m thick) surface salinity is stable above 6 ppt during winter. In fact, during winter, the level first-year ice microwave signatures change primarily due to snow cover related processes [Eppler et al., 1992]. The brightness temperature is directly affected by snow cover properties, e.g., liquid water content (W), grain size, density (ρ), and indirectly by the thermodynamic control of the snow cover on the ice, e.g., brine volume [Barber et al., 1995].

Multiyear ice has survived the seasonal melt. The melt processes re-crystallise the snow and ice, flush brine from the ice interior, and create surface topography, i.e., melt ponds and hummocks. The hummocks are porous with large air bubbles and voids, frozen melt ponds are less porous. Salinity increases downwards with about 0.0-0.1 ppt above sea level and 3.0-3.5 ppt below [Weeks and Ackley, 1986]. It differs from other ice types by a large number density of voids in the upper part of the ice, its low salinity, and its thickness (often several meters).

During summer (May-August), about half of the Arctic ice cover melts (its area shrinks from about $15{\cdot}10^6$ km^2 to $6.5{\cdot}10^6$ km^2) [Parkinson and Cavalieri, 1989]. Melting sea ice undergoes a significant and complex transformation described in connection with microwave remote sensing by e.g., Garrity [1992];

Gogineni et al. [1992]. These processes are understood relatively poorly in terms of microwave remote sensing signatures [Carsey et al., 1992]. The summer season is therefore beyond the scope of the present text, which focuses on winter conditions.

Sea ice emission modelling The emissivity model for sea ice with a snow cover developed in the project is described above (section 3.3.2).

3.4.2 Sensitivity of sea ice concentration estimates to surface emissivity

Current ice concentration algorithms use satellite microwave brightness temperatures between 6 and 89 GHz as input. The mean accuracies of some of the more common algorithms, used for SSM/I data, such as NASA Team [Cavalieri et al., 1984] and Bootstrap [Comiso, 1986] algorithms, are reported to be 1-6 % in winter [Steffen and Schweiger, 1991; Emery et al., 1994; Belchansky and Douglas, 2002]. At high ice concentrations, even small changes in the sea ice concentration have a significant impact on energy fluxes between the ocean and the atmosphere. Therefore, ice concentration is an important ice cover parameter to estimate accurately [Steffen and Schweiger, 1991].

The computed ice concentration accuracy is further degraded by particular atmospheric constituents like cloud liquid water, which can cause NASA Team ice concentration to erroneously increase by about 10 % [Oelke, 1997]. Changes in the surface emissivity, e, can depress the computed ice concentration by 20 % [Tonboe et al., 2003]. Toudal [1994] argued that variations in surface emissivity are a very important error source in sea ice concentration retrievals over consolidated ice from satellite passive microwave measurements.

The observed sensitivity of the different ice concentration algorithms using SSM/I satellite data, e.g., NASA Team, Bootstrap and Near 90 GHz [Svendsen et al., 1987] algorithms, to the atmosphere or surface brightness temperature is different as shown in Figure F-22 for a case in Baffin Bay. Coincident SAR images show that the real ice concentration in this area is stable above 94 % [Tonboe et al., 2003].

The sea ice emissivity normally varies during winter because of ice growth, snowfall, diurnal cycle and snow/ice metamorphism. Warm air outbreaks (Figure F-22) over the consolidated sea ice pack in Baffin Bay and Fram Strait/Arctic Ocean during winter offer a possibility to investigate the sensitivity of the ice concentration estimate to changes in the snow and ice cover emissivity in the course of days [Tonboe et al., 2003]. While the actual ice concentrations remain close to 100 % during and after the advection of warm air followed by snowfall and possibly rain, the formation of depth hoar and icy layers in the snow pack and in general the metamorphism accelerates as described in, e.g., Drinkwater et al. [1995]; Garrity [1992]. These winter warm air events may influence large areas (about 360 000 km^2) and, on a weekly timescale, smaller areas (15 000 km^2) along the ice edge [Tonboe et al., 2003; Voss et al., 2003].

The changes are persistent but recover in the course of months, e.g., the NASA Team ice concentration estimate is sensitive to layering in the snow pack and in particular to the air/snow dielectric contrast (i.e., density of the snow surface). Surface crusts with relatively high permittivity form during temporary warming (this strongly affects the NASA Team ice concentration), however new snow on top of the crust will decrease the dielectric contrast again thus reducing its influence on the brightness temperature. The NASA Team total ice concentration is robust to the simulated variations in the bottom snow layer correlation length.

The algorithm sensitivity to surface emissivity and thermometric temperature of the target depends on the selected polarisations and frequencies [Comiso et al., 1997; Emery et al., 1994; Toudal, 1994]. Emission models can be used to compute and analyse the sensitivity of the retrieved ice concentration to the microphysical properties of the snow and ice and to select and develop algorithms with low sensitivity to variations in the surface emissivity. Figure F-23 shows the modelled sensitivity of the NASA Team ice

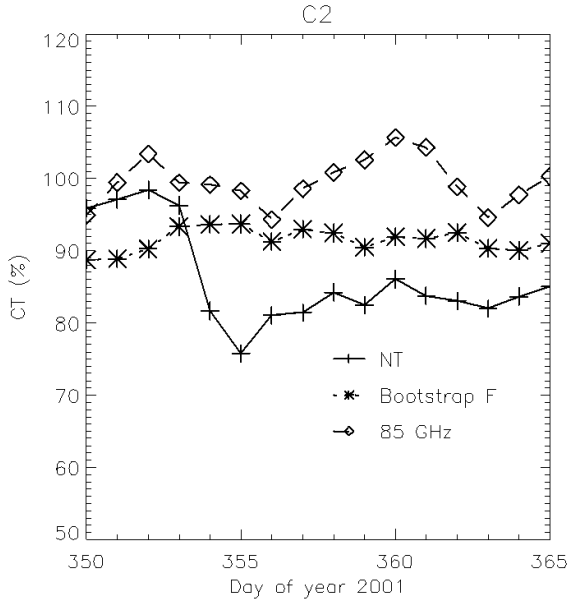

Figure F-22: *The satellite-observed average ice concentration in a small area in Baffin Bay (62.6° W, 71.5° N) using NASA Team (+), Bootstrap in frequency mode (∗) and Near 90GHz (◇) algorithms, December 2001. The variability is a function of ice concentration and both surface and atmospheric emissivity. The measured air temperature on a nearby meteorological station on the Greenland coast (Upernavik) increased above 0° C on day of year 353/354 and the freeze-up began on day 357 [from Tonboe et al., 2003].*

concentration to the density of the upper snow layer and correlation length of the bottom 1 cm snow layer.

Tonboe and Andersen [2004] made a model sensitivity study, using MEMLS, of nine common ice concentration algorithms where both the upper snow density and the bottom snow correlation length of a first-year ice profile were varied. The model simulations showed:

1. the combination of T_v (19 GHz) and T_v (37 GHz) as used in the Comiso Bootstrap algorithm in frequency mode, in the NORSEX [Svendsen et al., 1983] and in the Cal-val [Ramseier, 1991] algorithms has low sensitivity to the simulated emissivity changes,
2. algorithms also using T_h (the brightness temperature measured at horizontal polarisation) like Bristol [Smith, 1996], NASA Team and Bootstrap in polarisation mode are sensitive to the simulated density of the upper snow layer.

They further found that the simulated high sensitivity of the 89 GHz polarisation difference ($T_\mathrm{v} - T_\mathrm{h}$) to both density and the correlation length makes the algorithms using the high frequency channel like Near 90 GHz and TUD [Pedersen, 1998] very sensitive to the simulated snow cover emissivity. Mätzler et al. [1984] reported results from a field experiment that the high frequency (94 GHz) polarisation difference appeared insensitive to ice lenses at 7 cm depth in the snow. This observation was explained by strong attenuation and isotropic scattering in the upper snow layer. They further noted that "... at 94 GHz the surface reflectivity will lead primarily to polarisation effects ..." [Mätzler et al., 1984, p. 335]. The shallow penetration of the near 90 GHz microwaves (confined to the upper centimetres of the snow cover) means that different ice types with snow cover have similar radiative signatures. Furthermore, ice lenses below the upper centimetres of snow are only vaguely affecting the near 90 GHz emissivity. In other words, the near 90 GHz emissivity is largely insensitive to ice type and ice layers within the snow-pack,

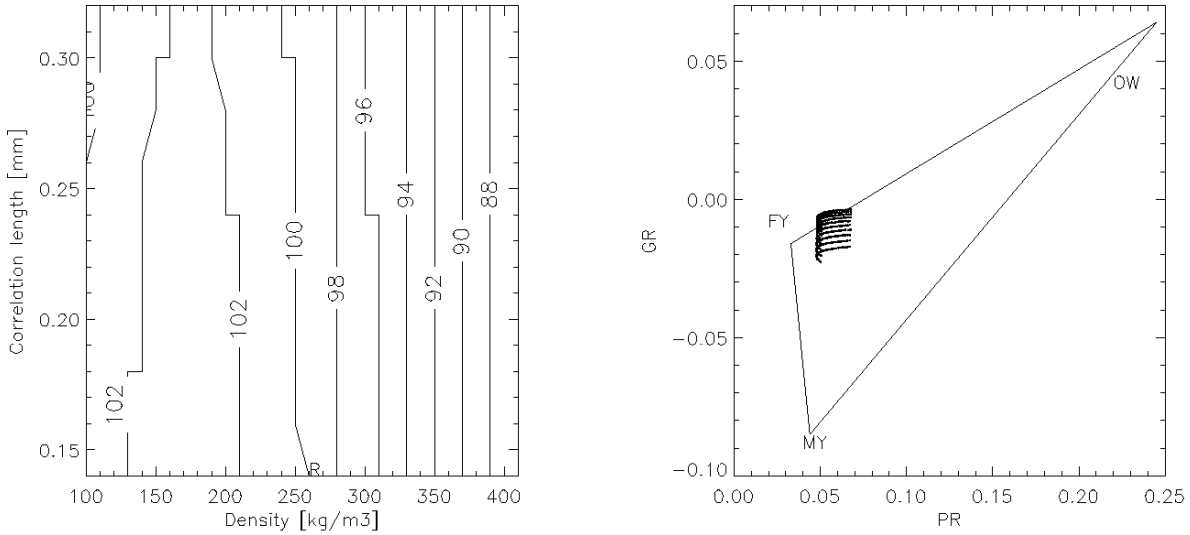

Figure F-23: *Simulated sensitivity at ground level of the NASA Team algorithm ice concentration [%] to variations in the upper snow layer density (layering) and bottom snow layer correlation length (grain size) in the snow cover on 100% first-year ice (left). Simulated data placed in the PR19 and GR19v/37v space with the approximate NASA Team retrieval triangle in the background (right). Tie-points for open water (OW), first-year ice (FY) and multiyear ice (MY) based on Andersen [1999] [from Tonboe and Andersen, 2004].*

which are affecting and complicating the interpretation of emissivity at, e.g., 19 and 37 GHz. These observations lead to the development of the Near 90 GHz ice concentration algorithm that exploits the higher spatial resolution at this frequency [Svendsen et al., 1987; Pedersen, 1998; Kaleschke et al., 2001]. However, the near 90 GHz polarisation difference is indeed sensitive to snow-ice surface emissivity. The model experiment indicates that the polarisation difference (at 89 GHz) increases as a function of air-snow dielectric contrast/reflectivity (upper snow layer density). The air-snow density contrast was not explicitly the theme of the laboratory experiment of Barber et al. [1998]. Even so, they note that as the snow cover permittivity increases: (1) e_{h} (90 GHz) decreases, (2) e_{v} is stable. This confirms our model experiments.

3.4.3 Ice concentration algorithms

A set of 7 passive microwave sea ice algorithms is considered in the following. We will only provide a brief description here. All algorithms, their acronyms and the channel combinations they use are given in Table T-12. Channels are referred to in terms of frequency in GHz and polarisation, which is either vertical or horizontal; the channel measuring at 19 GHz vertical polarisation is thus termed 19V.

It is noted that the Bootstrap algorithm is considered in its separate modes rather than following the exact specification which would require a switch between modes such that the polarisation mode (CP) is applied over consolidated ice and the frequency mode (CF) is used over loose ice and open water. The TUD algorithm is a hybrid approach that combines the CF with 85 GHz polarisation differences. At concentrations below a set threshold (currently 20%), it will return the CF result exclusively, whereas at higher ice concentrations the result is essentially the square root of the product of CF and scaled 85 GHz polarisation differences.

Table T-12: *Algorithms and acronyms used in the study*

Acronym	Algorithms	Channels
BRI	Bristol	19V, 19H, 37V, 37H
NT	NASA TEAM	19V,19H,37V
CF	Bootstrap frequency mode	19V,37V
CP	Bootstrap polarisation mode	37V,37H
NT2	NASA TEAM2	19V,19H,37V,37H,85V,85H
N90	Near 90 GHz algorithm	85V,85H
TUD	Technical University of Denmark hybrid	19V,37V,85V,85H

3.4.4 Validation study

An independent type of sea ice reference data is obtained from SAR data classified using a neural network approach similar to that used in Kern et al. [2003]. This basic framework was extended to handle RADARSAT and ENVISAT Wide Swath imagery and optimum texture feature sets were determined as described in Bøvith and Andersen [2005]. Experienced ice analysts of the Greenland Ice Service at DMI carried out selection of training data and assessment of the resulting classification. It is recognised that ambiguities in SAR imagery preclude the correct concurrent classification of all surface types within a given scene. Most frequently the return over wind-roughened water tends to be confused with ice, but the confusion between thin, low backscattering ice types and open water is in principle more serious. The approach taken is to accept these errors, and rely on the expertise of the ice analysts to mask out areas subject to misclassification. Emphasis was put on a correct classification of the sea-ice-covered area. Therefore, portions of a scene from the ice edge outward are often masked out. In practise this method, inside the mask, is thought to result in information consistent with a highly detailed ice chart. However, the special case of low backscattering ice and smooth open water is to a certain extent unrecoverable as even the trained specialist can hardly discern the two surface types in SAR imagery. These errors are a source of uncertainty, however, it is attempted to consistently classify such low backscatter surfaces as open water, such that a systematic bias towards over-representation of open water can be assumed to be the result. The resulting classified SAR image is collocated with SSM/I data, and ice concentration in a given SSM/I pixel overlap region can be derived as the simple ratio of SAR pixels classified as ice to the total number of SAR pixels within the overlap region. RADARSAT SCANSAR Wide scenes are averaged by a factor 2 to 100 m resolution, whereas ENVISAT ASAR Wide Swath mode scenes are retained at their nominal resolution of 75 m. This yields more than 60000 SAR pixels within a 25 km resolution SSM/I pixel and assures ample precision in the resulting concentration estimate. SAR scenes were ordered in 2003 and 2004 from locations well inside the ice edge and distributed geographically. A total of 68 scenes were analysed and 59 scenes were found to be useful after the classification and masking. Of the 9 rejected scenes, the reason for rejection was either that the proportion of the scene covered with sea ice was small or that the scene contained significant features that could not be identified unambiguously. The latter was encountered in a few cases when high winds caused open water to show as high backscatter features, precluding separation of leads and ridges. In general all seasons are reasonably well represented, when variations in ice extent are taken into account. The geographical coverage is illustrated in Figure F-24. In general there is a reasonable geographical balance, perhaps with a slight over-representation of the Laptev Sea during winter. It should be noted that we have applied a very conservative definition of winter and summer. Winter is the period from 31 October till 31 March while summer is defined as the period including June through September. This explains why the summer subset seemingly has thinner coverage.

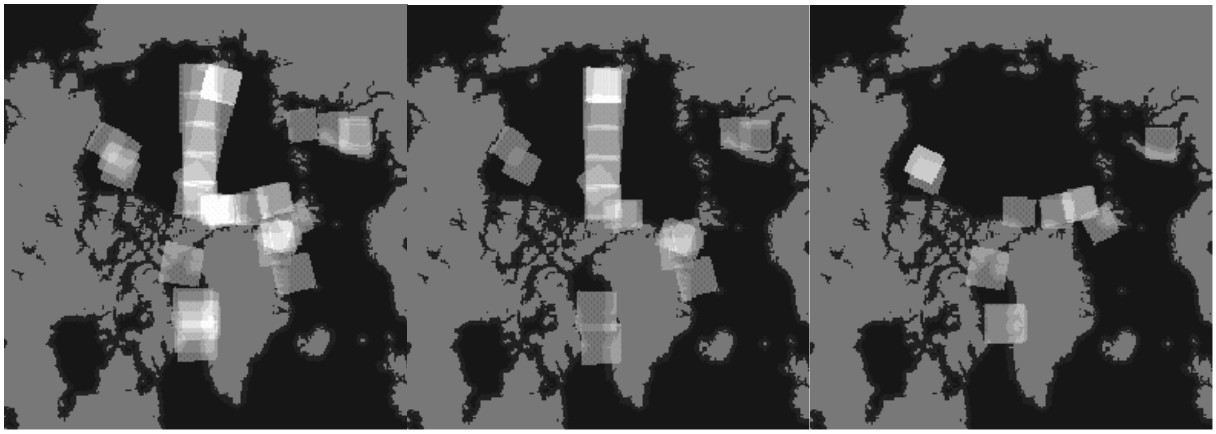

Figure F-24: *Geographical coverage of the SAR validation scenes: Total set (left); winter (centre); summer (right)*

3.4.5 Results

From the total data set, we initially analysed the correlation between SAR-based and SSM/I-based ice concentrations as a function of the SAR-based ice concentration. In general we obtain high correlations, around 0.9, at lower ice concentrations, which is very satisfactory. Interestingly the correlations drop off significantly at high ice concentration. This is in good accord with the results obtained from the comparison to RGPS (RADARSAT Geophysical Processor System) data, described in Andersen et al. [2005]. The statistics, given in Table T-13, shows that biases are in general less than 5% and vary much as expected, with NT and N90 underestimating the most. This is in agreement with findings by other authors [e.g. Comiso et al., 1997; Belchansky and Douglas, 2002; Meier, 2005] and for N90 it is the consequence of the fact that tie points were derived to match NT retrievals. The results for NT2 illustrate the problem of comparing algorithms at high ice concentration when retrievals are restricted to the physically meaningful interval. In general, the N90 and TUD algorithms are by far most sensitive to atmospheric influences. It is interesting to note that this is not reflected in the error standard deviations, indicating that for conditions found within the consolidated sea ice, the atmospheric influence is secondary to retrieval of sea ice total concentration.

Limiting the analysis to a subset of wintertime data (Table T-14), it is seen that the variability of the SAR ice concentrations is much reduced and the average concentration is found to be above 98 %. An obvious consequence is that the bias increases consistently with an increase in average SSM/I retrievals of typically 1-2%. The error standard deviations in relative terms vary approximately as for the full data set, however they are generally reduced by 1-3% with the exception CF and BRI. As expected in the high concentration regime, the correlations are vanishing for all algorithms. The primary error source in these comparisons is the existence of thin ice types whose radiative properties mimic a mixture of sea ice and water in most SSM/I algorithms and is highly ambiguous in the SAR data. Overall, we find that the variability of the SAR concentrations is significantly lower than that of the SSM/I retrievals. Recalling that the SAR concentrations favour high variability through the preferential classification of thin ice as open water, it implies that the variability of the SSM/I retrievals can hardly be explained by genuine sea ice concentration variability. The fact that the 85 GHz algorithms (N90, TUD) tend to report less variability indicates that atmospheric variability is not significant and suggests that emissivity variations are the primary influence.

Table T-13: *Results from the full SAR data set. "IC" means ice concentration. "NT2u" is a less constrained version of NT2 that does not crop ice concentrations above 100%. An "l" appended to "N90" and "TUD" signifies statistics computed from data averaged down to the resolution of the low frequency SSM/I channels.*

	Average IC [%]	Stdev [% IC]	No. obs.
SAR (low res.):	97.6529	9.01809	10084
SAR (high res.):	97.5833	9.77783	41012
	Bias [% IC]	Error Stdev [% IC]	Correlation
NT:	-4.405	10.086	0.613
NT2:	-1.078	7.006	0.759
NT2u:	5.200	9.507	0.685
CF:	0.746	9.915	0.647
CP:	-0.616	15.798	0.440
BRI:	0.237	10.192	0.625
N90l:	-3.685	7.881	0.729
N90:	-3.203	8.587	0.707
TUDl:	2.600	6.952	0.729
TUD:	3.067	7.611	0.706

Table T-14: *Same as Table T-13 but using only the winter subset*

	Average IC [%]	Stdev [% IC]	No. obs.
SAR (low res.):	98.5464	3.73111	5957
SAR (high res.):	98.5578	4.15613	24298
	Bias [% IC]	Error Stdev [% IC]	Correlation
NT:	-2.256	7.117	0.102
NT2:	0.067	4.872	0.069
NT2u:	7.053	7.189	0.094
CF:	2.361	7.622	0.080
CP:	-0.063	7.008	0.066
BRI:	1.459	6.305	0.091
N90l:	-2.282	6.101	0.133
N90:	-1.817	6.661	0.116
TUDl:	3.609	5.392	0.118
TUD:	4.045	5.846	0.099

3.4.6 Conclusions

The work on sea ice retrieval in IOMASA has followed both a theoretical path in the application of radiative transfer models to analyse effects of emissivity on sea ice retrievals and a more practical path with a comprehensive comparison between analysed SAR data and ice concentration retrievals. It was found that the main limiting factor to the further application of emissivity models in sea ice retrieval is the lack of knowledge of the sea ice and snow microphysical properties and in particular their typical vertical structures. From the practical comparisons, it was found that the algorithms with the shorter penetration depth, i.e., using mainly 85 GHz information, tend to produce significantly better statistics. During winter it was found that the variability in the reference field was consistently smaller than the variability of the passive microwave retrievals. The results provide a solid basis for the interpretation of

sea ice concentration retrievals not only in operational meteorological application that have been the scope of IOMASA, but also in climate and oceanographic applications. The results should have an impact on the future priorities of research. It is recommended to put emphasis on improved knowledge of snow on top of the sea ice but also to pay strong attention to synergies with alternative means of observing the sea ice.

3.5 Part 5: Demonstration of real-time processing and user interface

An Internet based distribution system for ice, weather and ocean information has been set up. The system provides near real time access to a large variety of data about the polar environment in a standard user environment. The system is freely available at: http://www.seaice.dk

Keywords: Satellite data, Microwave Radiometry, SAR, Information system, JAVA

3.5.1 Introduction

The amount of information available on the sea-ice, ocean and weather conditions for a particular region such as the Greenland Sea today is very large. However, the information is found in many different places, typically in incompatible formats that makes the task of optimally combining data into the desired set of information for a particular application very difficult. The applications vary from near real time usage for navigation, to off-line browsing of ice information for climate studies.

The task of this work thus was to process the information into common formats and build a browser that would allow user-defined views of the data. The Internet was the obvious data distribution medium and Java the programming language of choice because it allowed the generation of a tool that could be

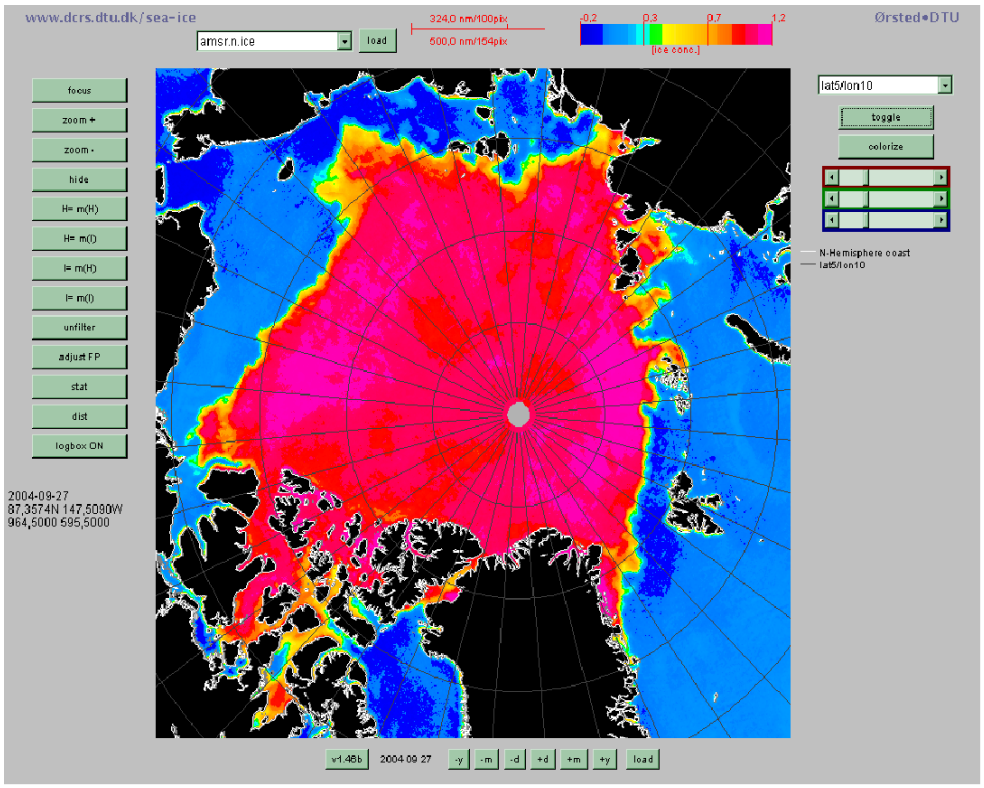

Figure F-25: *Example of AMSR-E ice concentration product in the DTU JAVA ice system.*

centrally maintained, and globally applied. Users will always get the latest version of the code. The JAVA run-time environment (Virtual Machine (VM)) is freely available from Sun Microsystems (http://java.sun.com) for most platforms.
Specific target groups for the browser are companies involved in planning and/or carrying out navigation in ice frequented waters, ice services in the Northern and Southern hemisphere, scientific partners in various EC projects etc.

3.5.2 Specification/requirements

The original purpose of the Java browser was to allow remote surveillance during off-hours and week-ends of the archive and product generation processes running at our central UNIX/Linux computer systems. The image visualisation software we had at the UNIX computers was built on top of software libraries that allow easy handling of images in different geometries and with different scales [Bagger et al., 1996]. A simple conversion to GIF and/or JPEG format would allow us to check the images using a Web-browser such as Netscape, but lacked the geometrical referencing of the UNIX software. The development of the Java browser showed great potential, and we decided to build an application that benefited from the geometrical knowledge of the UNIX software, the data compression capabilities of the GIF and JPEG image formats, and the transmission capabilities of the World Wide Web. The requirements to the system included the following:

Archive and Processing

- Downloading and archiving of relevant data from the Internet
  - ENVISAT ASAR GMM (Global Monitoring mode) data from ESA
  - AMSR-E data from NASA via the National Snow and Ice Data Center, U.S.
  - SSM/I data from Marshall Space Flight Center, U.S.
  - ERS-1/2 SAR data from ESA/ESRIN (not near real time)
  - Ice charts from the National Ice Center, U.S.
  - Wind and Wave forecasts from NCEP, U.S.
  - QuikSCAT scatterometer data from NOAA via the Danish Meteorological Institute
  - AMSU-A and AMSU-B data from the Cooperative Institute for Research in the Atmosphere (CIRA), Colorado State University, U.S.
  - SST (sea surface temperature) analysis data from NOAA, U.S.
  - SST and ice data from the EUMETSAT Ocean and Sea-Ice Satellite Application Facility (OSI-SAF)
  - MODIS data from NASA, U.S.
  - ATSR and AATSR data from ESA
  - Ice drift data from DTU, met.no, IFREMER and NCEP
- Processing of downloaded data into ice/weather/ocean relevant information
  - ENVISAT ASAR Global Monitoring mode data are converted to a polar stereographic grid. 1-day and 3-day mosaics are created, and 3-day ice drift fields are generated.
  - AMSR-E Processing for determination of ice, ocean and atmospheric fields (simple algorithms as well as the DTU optimal parameter estimation algorithm). Parameters are total ice concentration, multiyear ice fraction, atmospheric columnar water vapour, atmospheric columnar liquid water, SST, ice surface temperature, wind speed over the ocean.
  - QuikSCAT data are gridded into a polar stereographic projection.
  - SSM/I data processing, generation of contours and ice maps

  - NIC ice chart data are converted to DTU internal vector/polygon format
  - ERS SAR data mosaics of frames from same orbit etc.
  - MODIS data are converted to a polar stereographic projection
  - NOAA SST data are re-gridded into a polar stereographic projection
  - NCEP wind and wave forecasts are converted to the DTU internal vector format.

Browser

- Access to data archive via the Internet
- display of colour and grayscale satellite imagery
- display of colour-coded derived digital ice maps
- user-controlled colour & grayscale manipulation
- user-controlled zooming in & out
- latitude/longitude co-ordinates of any point at the click of the mouse
- user controlled addition of (vector) overlays showing
  - coastlines
  - latitude/longitude grids
  - bathymetry
  - contours of ice concentration
  - contours of ice concentration from past
  - contours of Ku-band (QuickSCAT) backscatter
  - other auxiliary data (cruise tracks, float tracks, SAR frames, ...)
- User controlled vector overlay colouring
- user controlled adjustment for simple registration errors
- combine data from different sensors
- combine data from different dates/times
- reasonable data transmission times, e.g., data compression of large files
- Platform independence or something that would work with most potential customers!
- Parameter values (such as temperature or ice concentration) at the click of the mouse
- Easy shift (shortcut) to another date

3.5.3 Implementation

Downloading and data archiving facility Data from various sources are acquired via FTP or HTTP and stored in a 'date tree' directory structure. All in-house processing is done using various scripts and utility programs.
Automatic download of AMSR-E, AMSU, ENVISAT ASAR GM and SSM/I data are carried out as data becomes available using automated FTP.
Offline, other types of data are added from CD-ROM (ERS SAR, ENVISAT ASAR WS, PRI, APP).

Pre-processing To produce images, the AMSR-E, AMSU, SSM/I, ASAR-GM, QuickSCAT and MODIS data are gridded into a polar stereographic projection. Various ice concentration products and ice indexes as well as some of the original SSM/I channels are created as images using default grayscale and pseudo colour tables. All images are in GIF or JPEG format for compression.
The SSM/I data are used to produce ice contour vectors at various concentrations (at 5, 15, 30, 60 and 90%).

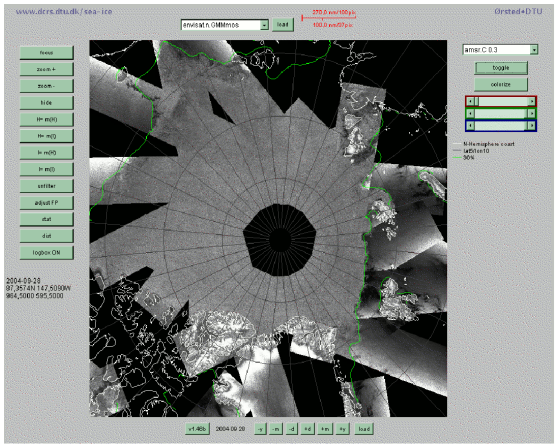

Figure F-26: *Example of ENVISAT ASAR Global Monitoring Mode mosaic in the DTU JAVA system.*

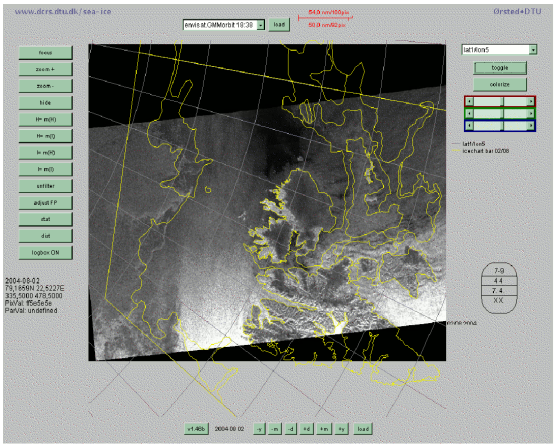

Figure F-27: *Example of clickable NIC ice chart overlaid an ENVISAT ASAR Global Monitoring mode image of the Svalbard area.*

ERS1/2 SAR and ENVISAT ASAR data are re-sampled to the polar stereographic projection and a vector-overlay showing the border of the SAR scene(s) is produced for referencing. Grayscale JPEG images are created. Various mosaics are created from the SAR images, and ice drift data are derived from the swath data (Walker et al, 2005).

Interactivity of the JAVA browser

User controlled selection and loading of images The browser defaults to the current day when loaded. It features a date control panel that allows the user to shift the date by one day, one month or one year. The available images from the day chosen are shown in a list, and the user can chose any image from the list for loading.

User controlled colour and grayscale manipulation To allow the user the possibility to enhance details in the image, four mapping filters are available. The user can adjust one parameter (either intensity or hue) as a function of another.
Two of the filters map from grey levels (black to white) (by adjusting intensity) and the other two map from blue through green and yellow to red (by adjusting hue).
This allows the user to, e.g., colourise a range of values from a grayscale image with the colours from blue to red, thereby enhancing small changes.
The range for the manipulation is selected by the user by pointing at two pixel values specifying the boundaries of the interval to be mapped.

Zooming and focusing The user can enlarge or shrink the image by zooming in or out. To examine part of a large image, its possible to focus on any part of an image effectively centering that part of the image for later zooming.

Latitude/Longitude co-ordinates For navigational purposes it is important to be able to get latitude/ longitude co-ordinates of any desired point in the image. This was originally implemented by downloading a grid file containing latitude/longitude co-ordinates of a set of grid points. This grid was then used

to linearly interpolate to the latitude/longitude co-ordinate of the desired point. However, it turned out that downloading the grid was rather time-consuming and not as flexible as we wanted, so we ended up implementing a set of map projection conversion routines that allows conversion from image co-ordinates to latitude/longitude. The run-time performance of the Java code is easily capable of these calculations.
At any time the user can click on a point in an image to get the corresponding latitude/longitude co-ordinates. This is accomplished by the projection information contained in the ASCII metadata file that is downloaded with the image.

Vector overlays The vector overlays are arranged in a list from which the user can select the 'actual overlay'. This overlay can then be toggled on and off and the RGB components of the overlay can be defined.
Current overlays available are:

- coastline,
- bathymetry (depth) curves at 200 m, 500 m, 1000 m,1500 m, 2000 m, and 3000 m etc.
- latitude/longitude grids at 1/1 1/5 5/10 degrees latitude/longitude spacing
- ice concentration curves derived from AMSR-E and SSM/I data at 5, 15, 30, 60 and 90% from a given date, three days ago and 7 days ago.
- Ice drift data from DTU, met.no, IFREMER and NCEP
- NIC clickable ice charts with display of "ice egg code" (World Meteorology Organization system for sea ice symbology)[3].
- QuickSCAT Ku-band backscatter contours
- ENVISAT and ERS SAR scene boundaries

Originally the overlays were downloaded in image co-ordinates (for performance reasons), but the performance of the Java code, and the implementation of map-projection code allows us to download vector overlays in latitude/longitude co-ordinates directly. The vector data files are all in ASCII format for easy generation and editing. A special run-length encoding has been developed as an alternative for larger vector files.

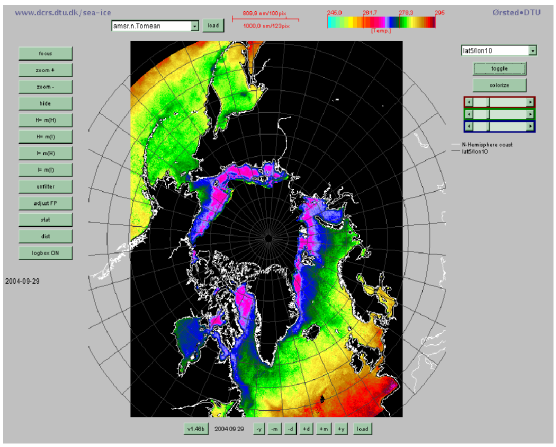

Figure F-28: *Example of a 7-day mean SST product derived from AMSR-E data.*

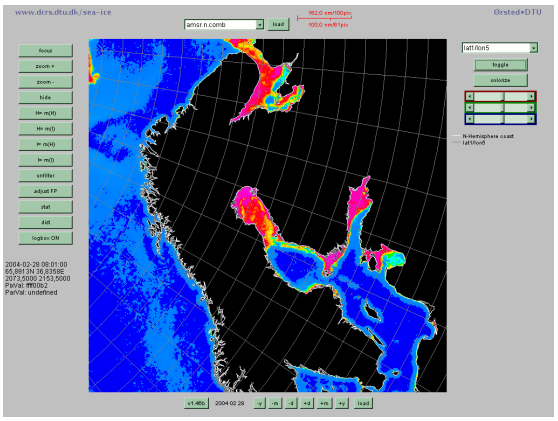

Figure F-29: *Example of a high resolution ice product for the Baltic Area.*

[3] see http://www.natice.noaa.gov/egg_code/index.html

3.5.4 Portability issues

Java is a platform-independent programming language, and very native to the Internet. This makes it a good choice for visualisation of image data across the World Wide Web. The browser has been tested with Netscape/Mozilla on a variety of platforms as well as with Internet Explorer under Windows.
Minor differences in the look of various buttons, scrollbars etc. are observed but the application generally works in all these environments.
For some additional functionality of the applet, Sun Microsystems JAVA applet viewer (comes with the Java software development kit) can be used, since it allows seamless resizing of the browser window.

3.5.5 Data transmission issues

By using GIF/JPEG/PNG images for representing visual data (images), a high compression ratio is obtained; also the images can be displayed on an ordinary web-page, for fast referencing.
By use of a World Wide Web browser that caches frequently used files, data-transmission rates are kept low.
Response time is good on a system that runs locally (Java) as opposed to CGI scripts that is run on remote servers. With CGI-scripts, performance degrades with server-load whereas on a Java system there is almost no waiting time after the data is transferred.

3.5.6 Conclusions

Advantages: The system provides a wealth of ice/weather and ocean information.
The archive (with the browser) can be copied to CD-ROM and work directly from there. This is a very useful feature for demonstrations.
Data transmission benefits from the caching of the web-browser. The structure of the data on our server means that the Java code only has to be downloaded once, and then will be readily available as long as it remains in the disk-cache of the client browser. The entire Java code that needs to be downloaded to run the browser is approx. 60 Kbytes (not including images etc.).
The entire system is free to use and can be found at http://www.seaice.dk

Off-line use: In order to make full use of the capabilities of the system, the user has to stay on-line for quite a long time, which may be expensive at satellite telecommunication rates from ship to shore.
For navigational use, under the constraints of expensive low bandwidth satellite communication, we offer the possibility of running the browser locally (on-board); keeping a local database that is updated at the beginning of a session by downloading one or more compressed files with the data for a specified region and period. Compressed data files for most regions of the Arctic and the Southern Oceans are being produced automatically for download and off-line use.

3.5.7 Appendices/Examples

Data exchange formats Data exchange formats for the most relevant data types have been defined as binary GRIB (gridded binary) format or HDF format for gridded data and plain ASCII format for more simple data.

Near real time data distribution to end-users A near real time data distribution system has been set up at DTU to present IOMASA results to interested parties. The server can be accessed through the IOMASA web portal at DTU: http://www.seaice.dk/iomasa

The IUP total water vapour algorithm has been implemented to run in near real time with the AMSU-B data stream at DTU. An example of the DTU water vapour retrieval from AMSR-E data is shown in Figure F-30 and the corresponding IUP water vapour from AMSU-B in Figure F-31.
The figures below show the layout of the system, and examples of retrievals of cloud liquid water (Figure F-30) and total atmospheric water vapour (Figure F-31):

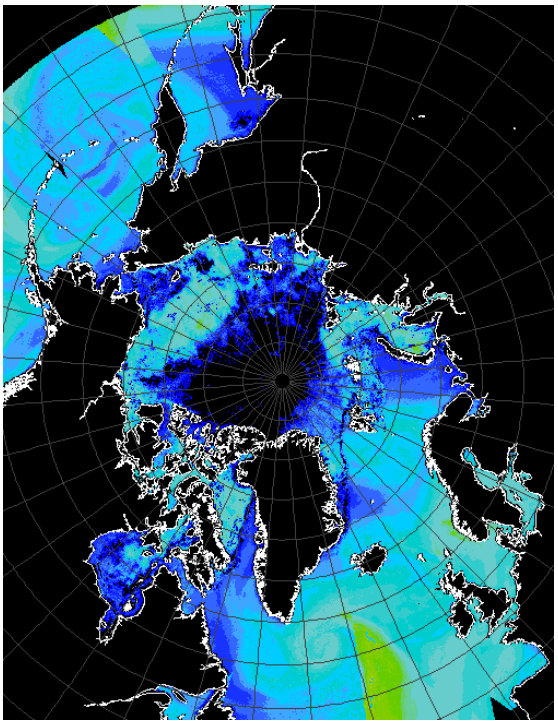

Figure F-30: *Retrieval of integrated water vapour using forward model from WP3. AMSR-E data from National Snow and Ice Data Center, December 5, 2004.*

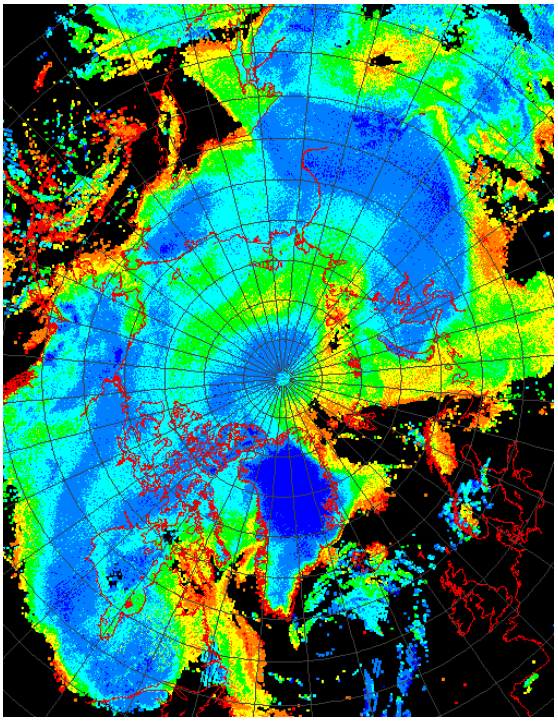

Figure F-31: *Retrieval of total atmospheric water vapour from AMSU-B data using University of Bremen algorithm from from WP1. AMSU-B data from Cooperative Institute for Research in the Atmosphere, Colorado State University, December 5, 2004.*

An AMSR-E parameter retrieval suite using an optimal estimation technique has been operationalized, and now runs in near real time with AMSR-E data from the National Snow and Ice Data Center (NSIDC). Data are distributed via the IOMASA web pages at DTU (http://www.seaice.dk/iomasa)
The retrievals are based on the atmosphere/ice/ocean forward emissivity/radiative transfer model of project part 3. The optimal estimation system has been used to demonstrate the applications of near real time retrievals of sea-ice, ocean and atmospheric parameters from satellite passive microwave observations.
Figure F-32 shows a suite of parameters as retrieved:
The IOMASA data distribution and visualisation system is based on tools developed in the IWICOS project (5^{th} framework IST project (IST-1999-11129). Figure F-33 shows an example of a Sea Surface Temperature field in the JAVA browser system.

3.5.8 Acknowledgement

The work at DTU has been carried out in connection with earlier projects under the 5th EU Framework programme. GreenICE (Contract no. EVK2-CT-2002-00156), IWICOS (Integrated Weather, Sea Ice and

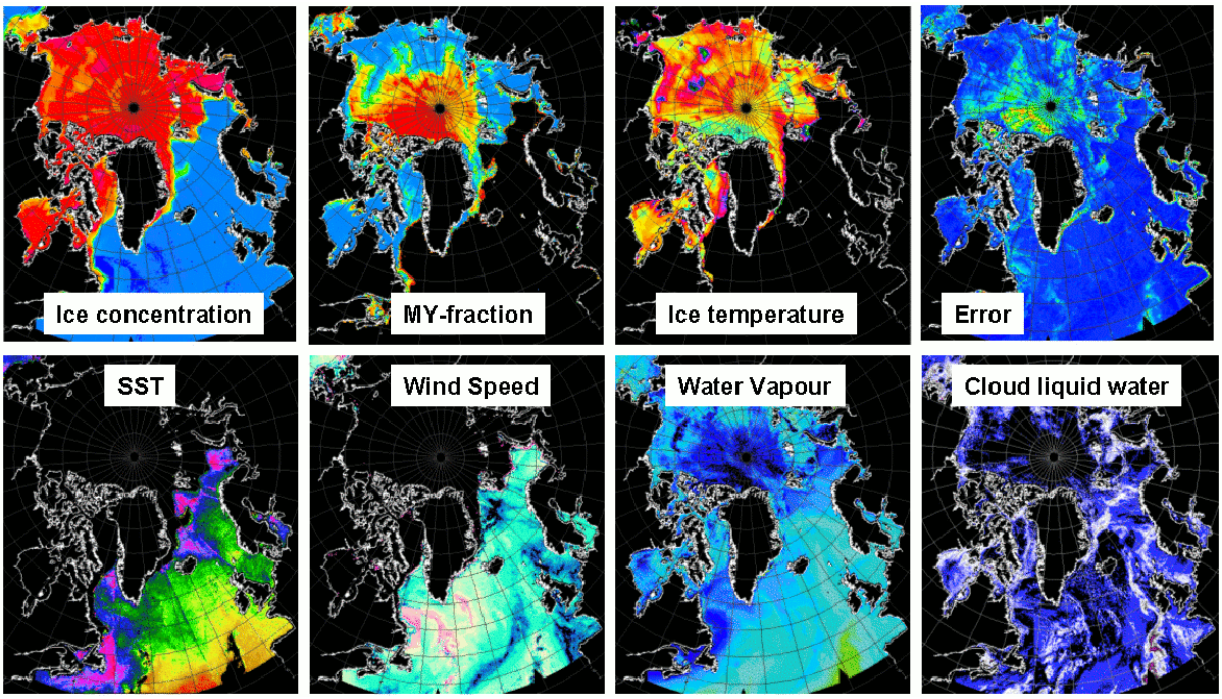

Figure F-32: *All parameters retrieved using the optimal parameter estimation technique. Input AMSR-E swath data from NSIDC, output the 7 parameters presented above. The plot titled Error shows the mismatch between the modelled and the measured antenna temperatures. Blue indicates very small errors, red large errors.*

Ocean Service System) (IST-1999-11129). We also wish to thank NASA for their open data policy that has allowed us to develop and succeed with this value adding service system. ESA is acknowledged for providing ERS-1 and ERS-2 and ENVISAT SAR data under PI projects AO2.DK103 and AOE-311
In addition we acknowledge partners in various earlier EC projects such as PELICON and SEALION, ESOP, ESOP2 and CONVECTION as well as the many other users for their valuable feedback which has helped us improve the system over the years.

4 Conclusions including socio-economic relevance, strategic aspects and policy implications

4.1 Summary

Part 1: Remote sensing of atmospheric parameters

An algorithm was adapted and extended that retrieves the total water vapour (TWV) content of the atmosphere from AMSU-B data. Below a TWV content of about 7 kg/m^2 (as is the case over most of the Arctic in winter), it is independent of the potentially unknown surface emissivity. Above 7 kg/m^2, it needs some bulk information about the surface emissivity and can then retrieve TWV with reduced accuracy. Assimilation of TWV data retrieved from AMSU-B data with this algorithm was implemented and tested in project part 2. An algorithm was developed and tested that retrieves surface emissivity at AMSU-A and -B window channels from AMSU data. It was used to determine typical emissivities of first-year and multiyear ice and to explore the scan angle dependence of surface emissivity. The R-factor, a cloud liquid

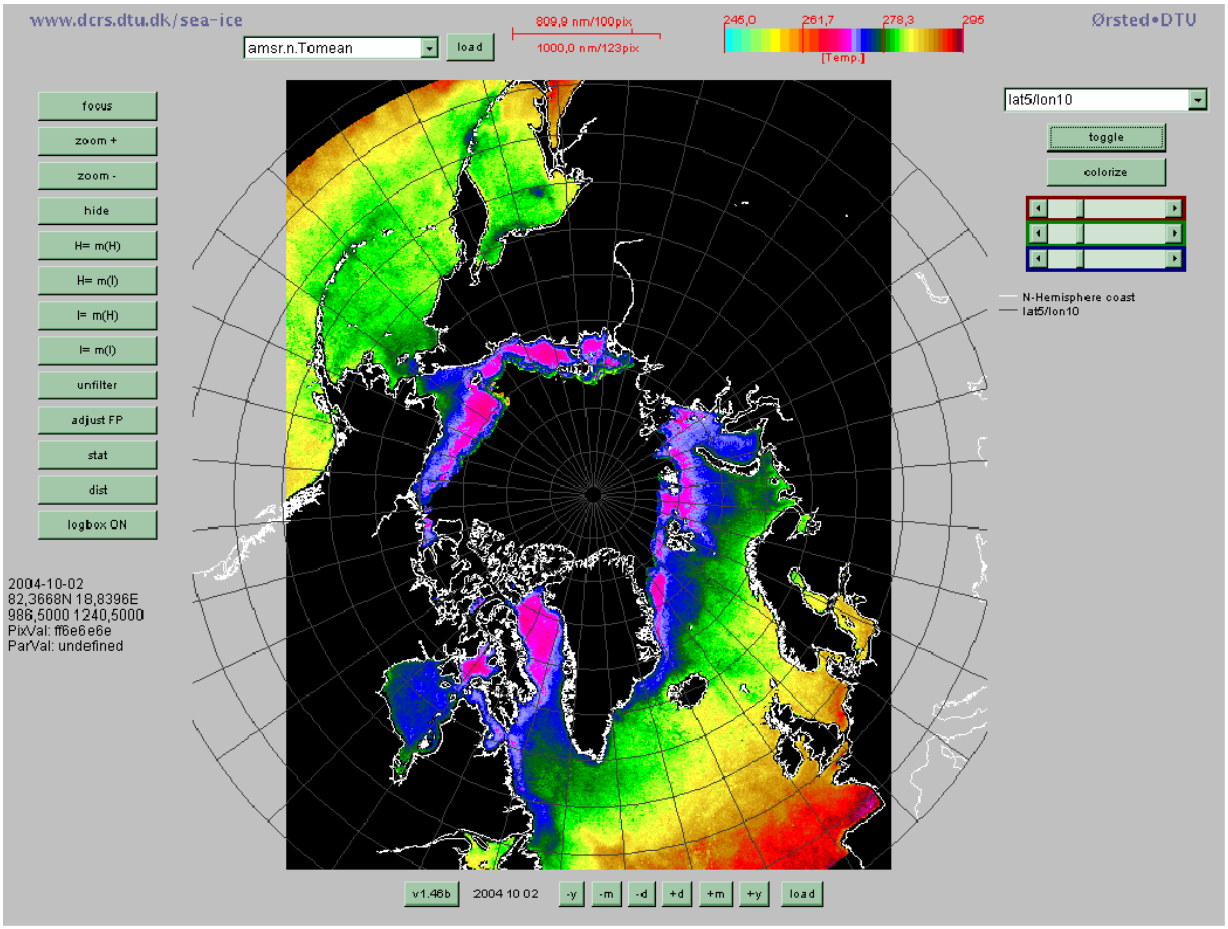

Figure F-33: *The daily SST composites are now being combined into a 7-day mean SST image for the northern hemisphere.*

water index, was tested as a tool for operational forecasters in order to locate fronts. Over open water, it provides valuable complementary information.

Part 2: Improving numerical weather prediction models

AMSU-A observations over sea ice were successfully assimilated in HIRLAM 3D-Var at the Norwegian Meteorological Institute. A new approach for estimating microwave sounding channel emissivity over sea ice was developed using information from the EUMETSAT OSI SAF. A quality control method developed specifically to handle asymmetric (cloud water) contamination was also developed. Assimilating AMSU-A observations over sea ice using the proposed approach had a positive effect on the mean sea level pressure and temperature profiles, especially in northern areas. Detailed impact studies strongly indicate benefits of adding AMSU-A observations over sea ice, and it should be planned to include this in operational model runs with HIRLAM.

The results from the validation of assimilation of TWV retrievals from AMSU-B show that the induced model changes remained in the Arctic region and mainly resulted in increased water vapour amount and cloudiness. This, in turn, led to a warmer model which produced better forecasts on temperature, mean sea level pressure and geopotential. In addition, validation of TWV assimilation pointed out an error in the HIRLAM system that was discovered thanks to the validation of the TWV – its correction in

the operational system reduced the bias in the 2 m temperature in the Arctic region by several degrees. The development of a new surface heat flux scheme lead to a significant improvement in forecasts of the potential temperature at lower model levels in the cases of moderate and very stable stratification in comparison with the conventional technique. There was also improvement for the vertical profile of wind in the boundary layer, for 2 meter temperature and humidity and for mean sea level pressure.

Part 3: Empirical model of emissivity and backscatter of sea ice

An empirical emissivity model has been established for both the AMSR-E microwave frequencies in the range from 6.9 to 89 GHz, and for the AMSU frequencies (23-183 GHz). The AMSU model has been implemented as a software module and integrated into the data assimilation scheme of met.no (project part 2) and the AMSR-E model has been used in a long term validation experiment in an optimal estimation algorithm at DTU (project part 5). A microphysical emissivity and backscatter model has been implemented and used in an extensive evaluation of sea ice concentration algorithms (project part 4) as well as in an assessment of the most important snow parameters influencing the emissivity of the ice/snow surface.

Part 4: Sea ice concentration retrieval

The work on sea ice retrieval in IOMASA has followed both a theoretical path in the application of radiative transfer models to analyse effects of emissivity on sea ice retrievals and a more practical path with a comprehensive comparison between analysed SAR data and ice concentration retrievals. It was found that the main limiting factor to the further application of emissivity models in sea ice retrieval is the lack of knowledge of the sea ice and snow microphysical properties and in particular their typical vertical structures. From the practical comparisons, it was found that the algorithms with the shorter penetration depth, i.e., using mainly 85 GHz information, tend to produce significantly better statistics. During winter it was found that the variability in the reference field was consistently smaller than the variability of the passive microwave retrievals. The results provide a solid basis for the interpretation of sea ice concentration retrievals not only in operational meteorological application that have been the scope of IOMASA, but also in climate and oceanographic applications. The results should have an impact on the future priorities of research. It is recommended to put emphasis on improved knowledge of snow on top of the sea ice but also to pay strong attention to synergies with alternative means of observing the sea ice.

Part 5: Real time processing and user interface

The Internet-based interactive distribution system (browser) provides a wealth of ice/weather and ocean information. The archive (with the browser) can be copied to CD-ROM and work directly from there. This is a very useful feature for demonstrations. Data transmission benefits from the caching of the web-browser. The structure of the data on our server means that the Java code only has to be downloaded once, and then will be readily available as long as it remains in the disk-cache of the client browser. The entire Java code that needs to be downloaded to run the browser is approx. 60 Kbytes (not including images etc.). The entire system is free to use and can be found at http://www.seaice.dk

4.2 European dimension

The project has brought together very different areas of expertise that, however, are necessary to achieve the objectives. The combination of

1. improved remote sensing of the polar surface above sea ice and open water,
2. improved atmospheric model results by assimilating the outcomes of point 1,
3. surface emissivity and backscatter models
4. improving the remote sensing of sea ice using the results of these 3 points

goes beyond the facilities of the involved individual institutes and has helped to increase our understanding of the Arctic environment. IOMASA has already resulted in improving NWP models and sea ice analyses. This project has complemented in an interdisciplinary way expertise and work being done nationally in the fields of

- remote sensing of the polar atmosphere (IUP)
- modelling and assimilation of the polar atmosphere (met.no and SMHI)
- modelling and retrieval of sea ice (DTU and DMI)

Thus, the project has helped to improve the coordination of a number of European national projects and has helped to fuse these into a Community-wide RTD programme. Finally the project has promoted the scientific cooperation and integration between European universities and research institutes and has contributed to transferring new technologies from research institutes (IUP and DTU) to operational services (DMI, met.no, and SMHI).

4.3 Contribution to Northern Dimension of the EU

The Northern Dimension is part of the EU's external and cross-border policies with a specific aim to raise the Union's profile in Northern Europe. The Northern Dimension builds upon the existing framework of contractual relationships, financial instruments and regional organisations without needing additional financial instruments in the EU.
Some of the methods developed in the project are on the way to their application in the operational environments of the weather services, e.g., the improved surface flux parameterisation (cf. section 3.2.8). Thus, this project is going to improve the weather forecasting infrastructure of countries throughout the European Arctic hence optimising the cost/benefit ratio of such services. It is in line with the policies of the Northern Dimension and contributes to their goals by various aspects:

- It has promoted the cooperation between the involved countries on environmental subjects affecting all of Northern Europe.
- The improved weather forecasts and sea ice analyses can help to increase prosperity and strengthen security in Northern Europe.
- The project has identified the interests of the EU in the North and has established a consistent line of action.
- The project has relied on the existing financial instruments of the EU (5th Framework Programme) and regional organisations, namely the national weather services and environmental research institutes of the involved countries.
- IOMASA has intensified the cooperation and increased the interaction between the actors of the region, EU member states and the Commission.
- The project has improved the interoperability of EU programmes (5th FP, Northern Dimension) as well as national research programmes with a view to creating synergies between them.

4.4 Widening of European scientific expertise

The project has broadened considerably the European expertise in the following fields:

- Remote sensing of the polar atmosphere

- Atmospheric modelling and assimilation
- Remote sensing and modelling of sea ice

Interrelations to ESA and EUMETSAT programmes

In addition to the objectives described above (cf. section 2, p. 3), IOMASA, by using SAR scenes for remote sensing of sea ice and evaluation of retrieval procedures, has contributed to the approved ENVISAT projects AO-170 (DTU, met.no), 287 and 311 (DMI), and 556 (IUP).
The research will enhance the value of data of meteorological European satellites because sensors similar to the sounders AMSU-A and -B are planned on the future METOP satellites. Therefore the project was also in line with the EUMETSAT policies.

5 Dissemination and exploitation of the results

5.1 Dissemination

Dissemination of the data is achieved by extending the interactive Internet-based user interface described above (cf. section 3.5, p. 47ff.) at http://www.seaice.dk/iomasa/ From the visitors to the that Web interface, the following groups of users of sea ice and atmospheric data have been identified:

- ship navigation, planning and administration of ship traffic
- export and import companies, producers and manufacturers
- exploration and expedition logistics
- oil, gas and offshore industry
- weather services and geophysical research
- consulting and service companies
- all groups of weather prediction users

5.2 Applications

The Improvements to NWP achieved during the project were developed and implemented to run in parallel to the operational environments of the project partners which at the same time are national weather services (DMI, met.no, SMHI).
Moreover, all weather services involved use the same NWP model (HIRLAM) for the project as well as for their operational forecasts. HIRLAM (High Resolution Local Area Model) is an international cooperation of the following meteorological institutes:

- Danish Meteorological Institute (DMI) (Denmark)
- Finnish Meteorological Institute (FMI) (Finland)
- Icelandic Meteorological Office (VI) (Iceland)
- Irish Meteorological Service (IMS) (Ireland)
- Royal Netherlands Meteorological Institute (KNMI) (The Netherlands)
- The Norwegian Meteorological Institute (met.no) (Norway)
- Spanish Meteorological Institute (INM) (Spain)
- Swedish Meteorological and Hydrological Institute (SMHI) (Sweden)
- Meteo-France (France, research cooperation)

A reference version of HIRLAM is maintained at the European Centre for Medium range Weather Forecasts (ECMWF), and all changes to HIRLAM are introduced via the reference system.

It is planned to bring the new assimilation schemes and the improved surface flux scheme into the HIRLAM reference system. This was also strongly encouraged by User Advisory Group member C. Fortelius, head of the atmospheric modelling group of the Finnish Meteorological Institute and member of the HIRLAM team. Thus, the progress achieved in the IOMASA can easily benefit to all HIRLAM member institutions.

The work on sea ice emissivity and concentration is taken up by the EUMETSAT OSI SAF.

6 Main literature produced

6.1 Refereed publications accepted:

G. Heygster, S. Andersen, N. Gustafsson, K. Kunzi, T. Landelius, H. Schyberg, L. Toudal (2002): IOMASA– Integrated Observation and Modeling of Arctic Sea ice and Atmosphere. *Proceedings of the 3rd EuroGOOS conference, Athens, 3-6 Dec. 2002.*

S. Sukoriansky, V. Perov, B. Galperin (2003): Application of a new spectral theory of turbulence to a stably stratified atmospheric boundary layer. *Geophysical Research Abstracts*, Vol. 5, 07037, 2003.

S. Sukoriansky, V. Perov, B. Galperin (2005): A spectral closure model for turbulent flows with stable stratification - Theory and a test case of atmospheric SBL over ice. *Boundary Layer Meteorology* Vol. 117(2), 237–251, 2005.

R. Tonboe, S. Andersen, L. Toudal, G. Heygster (2006): Sea ice emission modelling. Chapter in book *Thermal Microwave Radiation – Applications for Remote Sensing*, C. Mätzler, P.W. Rosenkranz, A. Battaglia and J.P. Wigneron (eds.), IEE Electromagnetic Waves Series, London, UK, in press, 2006.

6.2 Non-refereed publications:

R. Tonboe, S. Andersen, L. Toudal (2003): Anomalous winter sea ice backscatter and brightness temperatures. Danish Meteorological Institute Scientific Report 03-13, Copenhagen, 2003.

P. Dahlgren (2003): Ongoing and planned activities in the usage of ATOVS AMSU A/B in the HIRLAM 3DVAR system at SMHI. *Proceedings of ITSC-XIII, Montreal, Canada, November 2003.*

D. Hofman-Bang (2003): *Microwave remote sensing of sea ice.* Master Thesis, Denmark's Technical University, 2003.

R. Tonboe, S. Andersen (2004): Modelled radiometer algorithm ice concentration sensitivity to emissivity variations of the Arctic sea ice snow cover. Meteorological Institute Scientific Report 04-03, Copenhagen, 2004.

T. Bøvith, S. Andersen (2005): Sea ice concentration from Single polarized SAR data using second-Order Grey level Statistics and Learning Vector Quantization. Danish Meteorological Institute Scientific Report 05-04, Copenhagen, 2005. http://www.dmi.dk/dmi/sr05-04

S. Andersen, R. Tonboe, M. Lind, G. Heygster, C. Melsheimer, H. Schyberg, F. Tveter, P. Dahlgren, T. Landelius, N. Gustafsson (2005): IOMASA sea ice developments. Poster and paper at OSI SAF workshop March 15-17, 2005, Perros-Guirec, France.

P. Dahlgren (2005): Assimilation of ATOVS data at SMHI, Sweden. *Proceedings of ITSC-XIV, Beijing, China, May 2005.*

V. W. Thyness, L. Toudal Pedersen, H. Schyberg, F.T. Tveter (2005): Assimilating AMSU-A over Sea Ice in HIRLAM 3D-Var. *Proceedings of ITSC-XIV, Beijing, China, May 2005.*

C. Melsheimer, G. Heygster (2006): Retrieval of total water vapour from spacebourne microwave radiometer data. In *Reports on Polar Research* vol. 520/2006, Alfred-Wegener-Institut, Germany, 2006.

6.3 Refereed publications submitted:

R. Tonboe, S. Andersen, L. Toudal: On the surface melt induced sea ice emissivity changes around Greenland and the impact on the computed ice concentration using radiometer algorithms. Submitted to *Remote Sensing of Environment*, 2005.

S. Andersen, R. Tonboe, L. Kaleschke, G. Heygster, L. Toudal Pedersen: Intercomparison of passive microwave ice concentration retrievals over high ice concentration Arctic sea ice. Submitted to *J. Geophys. Res.*, 2005.

V. Perov, S. Sukoriansky, B. Galperin: Application of a new spectral theory of stably stratified turbulence to atmospheric boundary layer. Submitted to *Monthly Weather Review*, 2005.

References

S. Andersen. Monthly arctic sea ice signatures for use in passive microwave algorithms. In *Proc. EUMETSAT Meteorological Data Users Conference, 6-10 September 1999, Copenhagen*, 1999.

S. Andersen, R. Tonboe, and L. Kaleschke. Thorough validation of passive microwave ice concentration algorithms using classified SAR, ship observations and ice motion derived fields. *Submitted to J. Geophys. Res.*, 2005.

N. J. Bagger, L. T. Pedersen, H. Skriver, and P. Gudmandsen. Data analysis system for remote sensing data. In *Proc. 1st International Symposium about Scientific Imagery and Image Processing, Cannes 1995*, 1996.

D. Barber, A. K. Fung, T. C. Grenfell, S. V. Nghiem, R. G. Onstott, V. I. Lytle, D. K. Perovich, and A. J. Gow. The role of snow on microwave emission and scattering over first-year sea ice. *IEEE Trans. Geosci. Remote Sens.*, 36(5):1750–1763, 1998.

D. G. Barber, S. P. Reddan, and E. F. LeDrew. Statistical characterisation of the geophysical and electrical properties of snow on landfast first-year sea ice. *J. Geophys. Res.*, 100(C2):2673–2686, 1995.

G. I. Belchansky and D. C. Douglas. Seasonal comparisons of sea ice concentration estimates derived from SSM/I, OKEAN, and RADARSAT data. *Remote Sens. Environ.*, 81:67–81, 2002.

L. Breivik, S. Eastwood, O. Godoy, H. Schyberg, S. Andersen, and R. Tonboe. Sea Ice Products for EUMETSAT satellite application facility. *Can. J. Remote Sens.*, 27:403–410, 2001.

S. Buehler, P. Eriksson, T. Kuhn, A. von Engeln, and C. Verdes. ARTS, the atmospheric radiative transfer simulator. *J. Quant. Spectroscopy and Radiative Transfer*, 91:65–93, 2005. doi: 10.1016/j.jqsrt.2004.05.051.

T. Bøvith and S. Andersen. Sea ice concentration from single-polarized SAR data using second-order grey level statistics and learning vector quantization. Scientific Report 05-04, Danish Meteorological Institute, 2005.

F. D. Carsey, editor. *Microwave Remote Sensing of Sea Ice*. Geophysical monograph no. 68. American Geophysical Union, Washington, DC, 1992.

F. D. Carsey, R. G. Barry, D. A. Rothrock, and W. F. Weeks. Status and future directions for sea ice remote sensing. In Carsey [1992], pages 444–446.

D. Cavalieri, P. Gloersen, and W. J. Cambell. Determination of sea ice parameters with the NIMBUS 7 SMMR. *J. Geophys. Res.*, 89(D4):5355–5369, 1984.

J. Comiso. Characteristics of arctic winter sea ice from satellite multispectral microwave observations. *J. Geophys. Res.*, 91(C1):975–994, 1986.

J. Comiso, D. J. Cavalieri, C. L. Parkinson, and P. Gloersen. Passive microwave algorithms for sea ice concentration: a comparison of two techniques. *Remote Sens. Environ.*, 60:357–384, 1997.

M. R. Drinkwater, R. Hosseinmostafa, and P. Gogineni. C-band backscatter measurements of winter sea ice in the Weddell sea, Antarctica. *Int. J. Remote Sens.*, 16(17):3365–3389, 1995.

R. Elliot and G. Gaffen. On the utility of radiosonde humidity archives for climate studies. *Bull. Am. Meteorol. Soc.*, 72:1507–1520, 1991.

W. J. Emery, C. Fowler, and J. Maslanik. Arctic sea ice concentrations from Special Sensor Microwave Imager and Advanced Very High Resolution Radiometer satellite data. *J. Geophys. Res.*, 99(C9): 18329–18342, 1994.

S. English and T. Hewison. A fast generic millimetre wave emissivity model. *Proceedings of SPIE*, 3503: 288–300, 1998.

D. Eppler et al. Passive microwave signatures of sea ice. In Carsey [1992], pages 47–71.

R. Fuhrhop, T. C. Grenfell, G. Heygster, K.-P. Johnson, P. S. M. Schrader, and C. Simmer. A combined radiative transfer model for sea ice, open ocean and atmosphere. *Radio Sci.*, 33(2):303–316, March-April 1998.

C. Garrity. Characterisation of snow on floating ice and case studies of brightness temperature changes during the onset of melt. In Carsey [1992], pages 313–328.

S. P. Gogineni, R. K. Moore, T. C. Grenfell, D. G. Barber, S. Digby, and M. Drinkwater. The effects of freeze-up and melt processes on microwave signatures. In Carsey [1992], pages 329–341.

T. J. Hewison and S. J. English. Airborne retrievals of snow and ice surface emissivity at millimeter wavelengths. *IEEE Trans. Geosci. Remote Sens.*, 37(4):1871–1879, 1999.

M. Janssen, editor. *Atmospheric Remote Sensing by Microwave Radiometry*. John Wiley and Sons, New York, 1993. 572 pp.

L. Kaleschke, C. Lüpkes, T. Vihma, J. Haarpaintner, A. Bochert, J. Hartmann, and G. Heygster. Sea ice remote sensing for mesoscale ocean-atmosphere interaction analysis. *Canadian Journal of Remote Sensing*, 27(5):526–537, 2001.

S. Kern, L. Kaleschke, and D. Clausi. A comparison of two 85GHz SSM/I ice concentration algorithms with AVHRR and ERS-2 SAR imagery. *IEEE Trans. Geosci. Remote Sens.*, 41(10):2294–2306, 2003.

M. Klein, A. J. Gasiewski, D. J. Cavalieri, and T. Markus. Meltpond2000 polarimetric scanning radiometer sea ice brightness temperatures. Technical report, National Snow and Ice Data Center, Boulder, CO, USA, 2004.

W. Meier. Comparison of passive microwave ice concentration algorithm retrievals with AVHRR imagery in Arctic peripheral seas. *IEEE Trans. Geosci. Remote Sens.*, 43(6):1324–1337, 2005.

J. Miao. *Retrieval of Atmospheric Water Vapor Content in Polar Regions Using Spaceborne Microwave Radiometry*. Reports on Polar Research 289/1998. Alfred-Wegener Institute for Polar and Marine Research, Bremerhaven, Germany, 1998. 109 pp.

J. Miao, T. Markus, and A. Burns. Retrieval of temperature profiles over sea ice with multi-sensor analysis: Combination of the DMSP's SSM/I, OLS, and SSM/T1 sensors. In *Proceed. 1995 International Geoscience and Remote Sensing Symposium, Florence, Italy, 10-14 July*, pages 1142–1143, 1995.

J. Miao, K. Johnsen, S. Kern, G. Heygster, and K. Künzi. Signature of clouds over Antarctic sea ice detected by the Special Sensor Microwave/Imager. *TGARSS*, 38(5):2333–2344, September 2000.

J. Miao, K. F. Künzi, G. Heygster, T. A. Lachlan-Cope, and J. Turner. Atmospheric water vapor over Antarctica derived from SSM/T2 data. *J. Geophys. Res.*, 106(D10):10187–10203, 2001.

C. Mätzler. Applications of the interaction of microwaves with the natural snow cover. *Remote Sensing Reviews*, 2(2):259–391, 1987.

C. Mätzler. Relation between grain-size and correlation length of snow. *Journal of Glaciology*, 48(162): 461–466, 2002.

C. Mätzler and A. Wiesmann. Extension of the microwave emission model of layered snowpacks to coarse grained snow. *Remote Sens. Environ.*, 70:317–325, 1999.

C. Mätzler, R. O. Ramseier, and E. Svendsen. Polarisation effects in sea ice signatures. *IEEE Journal of Oceanic Engineering*, OE-9(5):333–338, 1984.

C. Mätzler, A. Wiesmann, J. Pulliainen, and M. Hallikainen. Development of microwave emission models of snowpacks. In C. Mätzler, editor, *Radiative transfer models for microwave radiometry*, pages 105–116. European Commission COST Action 712, final report, 2000.

S. V. Nghiem, R. Kwok, S. H. Yueh, and M. R. Drinkwater. Polarimetric signatures of sea ice - 1. theoretical model. *JGR*, 100(C7):13665–13679, 1995.

C. Oelke. Atmospheric signatures in sea-ice concentration estimates from passive microwaves: modelled and observed. *Int. J. Remote Sens.*, 18(5):1113–1136, 1997.

C. L. Parkinson and D. J. Cavalieri. Arctic sea ice 1973-1987: seasonal, regional, and interannual variability. *J. Geophys. Res.*, 94(C10):14499–14523, 1989.

L. Pedersen. Chapter 6.2. In S. et al, editor, *IMSI report no. 8. Development of new satellite ice data products*, number 145. Nansen Environmental and Remote Sensing Center, Bergen, Norway, 1998.

C. Prigent, F. Chevallier, F. Karbou, P. Bauer, and G. Kelly. AMSU-A land surface emissivity estimation for numerical weather prediction. Technical report, EUMETSAT, NWP SAF, 2004. document no. NWPSAF-EC-TR-009.

R. Ramseier. Sea ice validation. In J. Hollinger, editor, *DMSP special sensor microwave/imager calibration/validation*. Naval Research Laboratory, Washington, DC, 1991.

P. W. Rosenkranz. Retrieval of temperature and moisture profiles from AMSU-A and AMSU-B measurements. *TGARSS*, 39(11):2429–2435, 2001.

R. Saunders and P. Brunel. RTTOV-7 - technical report. Technical report, EUMETSAT, NWP SAF, 2002. NWPSAF-MO-TR-009. Available at http://www.metoffice.com/research/interproj/nwpsaf/rtm/rttov7_tr.pdf.

H. Schyberg, T. Landelius, S. Thorsteinsson, F. Tveter, O. Vignes, B. Amstrup, N. Gustafsson, H. Järvinen, and M. Lindskog. Assimilation of ATOVS data in the HIRLAM 3D-Var system. HIRLAM technical report no. 60, HIRLAM Project, 2003. Available from HIRLAM-5 Project c/o Per Undén, SMHI, S-60176 Norrköping, Sweden.

N. Selbach. *Determination of Total Water Vapour and Surface Emissivity of Sea Ice at 89 GHz, 157 GHz and 183 GHz in the Arctic winter*. Berichte aus dem Institut für Umweltphysik, Vol. 21. Logos-Verlag, Berlin, Germany, 2003. PhD thesis, 191 pp.

M. Shokr. Field observations and model calculations of dielectric properties of Arctic sea ice in the microwave C-band. *IEEE Trans. Geosci. Remote Sens.*, 36(2):463–478, 1998.

D. Smith. Extraction of winter sea-ice concentration in the Greenland and Barents Seas from SSM/I data. *IJRS*, 17(13):2625–2646, 1996.

K. Steffen and A. Schweiger. NASA team algorithm for sea ice concentration retrieval from Defence Meteorological Satellite Program Special Sensor Microwave Imager: comparison with Landsat satellite imagery. *J. Geophys. Res.*, 96(C12):21971–21987, 1991.

S. Surdyk and M. Fily. Comparison of the passive microwave spectral signature of the Antarctic ice sheet with ground traverse data. *Annals of Glaciology*, 17:161–166, 1993.

E. Svendsen, K. Kloster, B. Farelly, O. M. Johannesen, J. A. Johannesen, W. J. Campbell, P. Gloersen, D. J. Cavalieri, and C. Mätzler. Norwegian remote sensing experiment: Evaluation of the Nimbus 7 Scanning Multichannel Microwave Radiometer for sea ice research. *J. Geophys. Res.*, 88(C5):2781–2791, 1983.

E. Svendsen, C. Mätzler, and T. Grenfell. A model for retrieving total sea ice concentration from spaceborne dual-polarized passive microwave instrument operating near 90 GHz. *Int. J. Remote Sens.*, 8(10): 1479–1487, 1987.

R. Tonboe, S. Andersen, L. Toudal, and G. Heygster. Sea ice emission modelling applications. In C. Mätzler, P. Rosenkranz, A. Battaglia, and J. Wigneron, editors, *Thermal Microwave Radiation - Applications for Remote Sensing*, IEE Electromagnetic Waves Series. IEE,London, UK, 2005. In press 2005/6.

R. T. Tonboe and S. Andersen. Modelled radiometer algorithm ice concentration sensitivity to variations of the Arctic sea ice snow cover. Scientific Report 04-03, Danish Meteorological Institute, 2004. 34 pp.

R. T. Tonboe, S. Andersen, and L. Toudal. Anomalous winter sea ice backscatter and brightness temperatures. Scientific Report 03-13, Danish Meteorological Institute, 2003. 59 pp.

L. Toudal. Merging microwave radiometer data and meteorological data for improved sea ice concentrations. *EARSeL Advances in Remote Sensing*, 3(2 XII):81–89, 1994.

W. B. Tucker, T. C. Grenfeld, R. G. Onstott, D. K. Perovich, A. J. Gow, R. A. Shuchman, and L. Sutherland. Microwave and physical properties of sea ice in the winter marginal ice zone. *J. Geophys. Res.*, 96(C3):4573–4587, 1991.

F. Tveter. On optimal observation quality control theory for numerical weather prediction systems. Norwegian meteorological institute note no. 7/2005, Norwegian Meteorological Institute, 2005. Available from the Norwegian Meteorological Institute, http://www.met.no, P.O.Box 43 Blindern, NO-0313 Oslo, Norway.

F. T. Ulaby and W. H. Stilles. The active and passive microwave response to snow parameters: 2. Water equivalent of dry snow. *J. Geophys. Res.*, 85(C2):1045–1049, 1980.

F. T. Ulaby, R. K. Moore, and A. K. Fung. *Microwave Remote Sensing, From Theory to Applications, vol. 3*. Artech House, Dedham, MA, 1986.

S. Voss, G. Heygster, and R. Ezraty. Improving the sea ice type discrimination by the simultaneous use of SSM/I and scatterometer data. *Polar Research*, 22(1):35–42, 2003.

W. F. Weeks and S. F. Ackley. The growth, structure and properties of sea ice. In N. Untersteiner, editor, *The geophysics of sea ice*, pages 9–164. Plenum, New York, 1986.

F. Weng, L. Zhao, R. Ferraro, G. Poe, X. Li, and N. Grody. Advanced Microwave Sounding Unit cloud and precipitation algorithms. *Radio Sci.*, 38(4), 2003. doi: 10.1029/2002RS002679.

F. J. Wentz and T. Meissner. AMSR Ocean Algorithm. Algorithm Theoretical Basis Document (ATBD). version 2, Remote Sensing Systems, California, U.S., 2 November, 2002.

A. Wiesmann and C. Mätzler. Microwave emission model of layered snowpacks. *Remote Sens. Environ.*, 70:307–316, 1999.

D. P. Winebrenner, J. Bredow, A. K. Fung, M. R. Drinkwater, S. Nghiem, A. J. Gow, D. K. Perowich, T. C. Grenfell, H. C. Han, J. A. Kong, J. K. Lee, S. Mudaliar, R. G. Onstott, L. Tsang, and R. D. West. Microwave sea ice signature modelling. In Carsey [1992], pages 137–175.

List of Tables

List of Figures

Abbreviations/Acronyms

3DVar	Three-Dimensional Variational Analysis
AAPP	ATOVS and AVHRR Processing Package
AHVRR	Advanced Very High Resolution Radiometer
ADEOS	Advanced Earth Observing Satellite
AMSR	Advanced Microwave Scanning Radiometer; on satellite ADEOS-2 (Midori)
AMSR-E	Advanced Microwave Scanning Radiometer for EOS; on satellite Aqua
AMSU	Advanced Microwave Sounding Unit; on NOAA satellites
CLW	cloud liquid water
CMIS	Conical Microwave Imager Sounder
DMI	Danish Meteorological Institute
DMSP	Defence Meteorological Satellite Program (U.S.A.)
DTU-DCRS	Technical University of Denmark
ECMWF	European Centre for Medium-Range Weather Forecast
ERS	European Remote sensing Satellite
FY	first-year (ice)
GRIB	gridded binary (format)
HIRLAM	High Resolution Limited Area Model
HIRVDA	HIRLAM variational data assimilation
Ifremer	Institut Français pour la Recherche et l'Exploitation de la Mer
ISBA	Interactions between Surface–Biosphere–Atmosphere
IUP	Institut für Umweltphysik (Institute of Environmental Physics)
LES	large eddy simulation
MEMLS	Microwave Emission Model for Layered Snow-packs
met.no	The Norwegian Meteorological Institute
MSLP	mean sea level pressure
MY	multiyear (ice)
NASA	National Aeronautics and Space Administration (U.S.A.)
NCEP	National Centers for Environmental Prediction (U.S.A.)
NSCAT	NASA SCATterometer
NOAA	National Oceanic and Atmospheric Administration (U.S.A.)
NSIDC	National Snow and Ice Data Center
NWC SAF	Satellite Application Facility (SAF) on Support to Nowcasting and Very Short Range Forecasting
NWP	numerical weather prediction
NWP SAF	Satellite Application Facility (SAF) on Numerical Weather Prediction
OSI SAF	Satellite Application Facility (SAF) on Ocean and Sea Ice
SAR	synthetic aperture radar
SMHI	Swedish Meteorological and Hydrological Institute
SMOS	Soil Moisture and Ocean Salinity
SSM/I	Special Sensor Microwave/Imager on DMSP satellites
SSMIS	Special Sensor Microwave Imager/Sounder on DMSP satellites
SSM/T	Special Sensor Microwave/Temperature sounder on DMSP satellites
SST	sea surface temperature
TWV	total water vapour
UAG	User Advisory Group
DTU	Technical University of Denmark

DMI	Danish Meteorological Institute
UB	University of Bremen